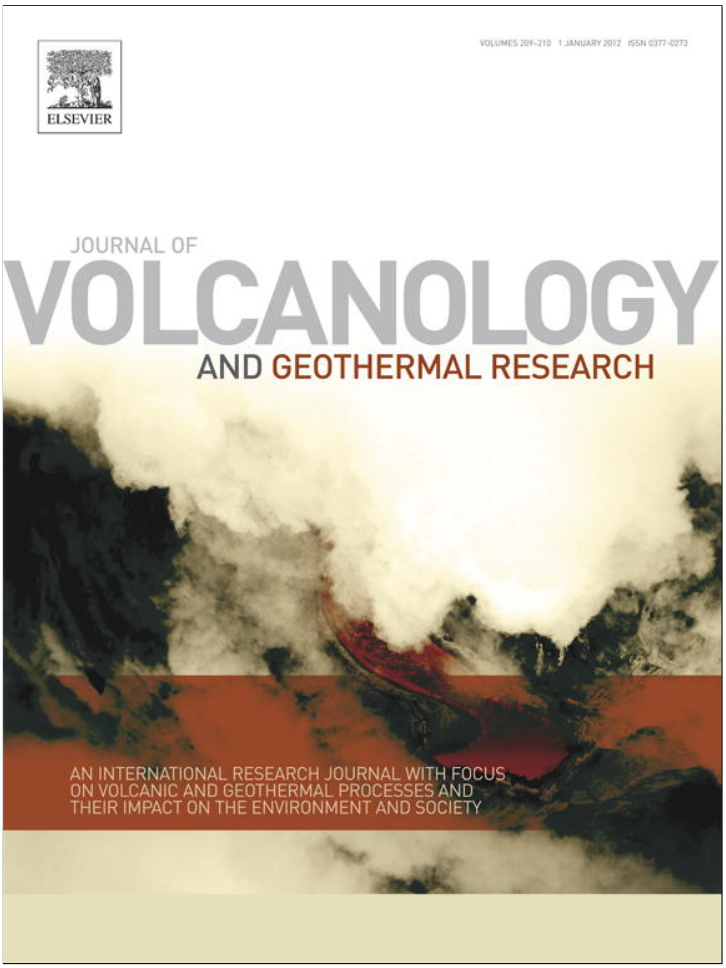

(This is a sample cover image for this issue. The actual cover is not yet available at this time.)

Journal of Volcanology and Geothermal Research 225–226 (2012) 13–29

Contents lists available at SciVerse ScienceDirect

Journal of Volcanology and Geothermal Research

journal homepage: www.elsevier.com/locate/jvolgeores

Petrochemistry of a xenolith-bearing Neogene alkali olivine basalt from northeastern Iran

Saeed Saadat [a,b,*], Charles R. Stern [a]

[a] Department of Geological Sciences, University of Colorado, Boulder, USA
[b] Department of Geological Sciences, Mashhad Branch, Islamic Azad University, Mashhad, Iran

ARTICLE INFO

Article history:
Received 8 July 2011
Accepted 20 February 2012
Available online 3 March 2012

Keywords:
Iran
Lut block
Basalt
Peridotite xenoliths
Plagioclase megacryst

ABSTRACT

A small isolated Neogene, possibly Quaternary, monogenetic alkali olivine basalt cone in northeastern Iran contains both mantle peridotite and crustal gabbroic xenoliths, as well as plagioclase megacrysts. The basaltic magma rose to the surface along pathways associated with local extension at the junction between the N–S right-lateral and E–W left-lateral strike slip faults that form the northeastern boundary of the Lut microcontinental block. This basalt is enriched in LREE relative to HREE, and has trace-element ratios similar to that of oceanic island basalts (OIB). Its $^{87}Sr/^{86}Sr$ (0.705013 to 0.705252), $^{143}Nd/^{144}Nd$ (0.512735 to 0.512738), and Pb isotopic compositions all fall in the field of OIB derived from enriched (EM-2) mantle. It formed by mixing of small melt fractions from both garnet-bearing asthenospheric and spinel-facies lithospheric mantle. Plagioclase (An_{26-32}) megacrysts, up to 4 cm in length, have euhedral crystal faces and show no evidence of reaction with the host basalt. Their trace-element concentrations suggest that these megacrysts are co-genetic with the basalt host, although their $^{87}Sr/^{86}Sr$ (0.704796) and $^{143}Nd/^{144}Nd$ (0.512687) ratios are different than this basalt. Round to angular, medium-grained granoblastic meta-igneous gabbroic xenoliths, ranging from ~1 to 6 cm in dimension, are derived from the lower continental crust. Spinel–peridotite xenoliths equilibrated in the subcontinental lithosphere at depths of 30 to 60 km and temperatures of 965 °C to 1065 °C. These xenoliths do not preserve evidence of extensive metasomatic enrichment as has been inferred for the mantle below the Damavand volcano further to the west in north-central Iran, and clinopyroxenes separated from two different mantle xenoliths have $^{87}Sr/^{86}Sr$ (0.704309 and 0.704593) and $^{143}Nd/^{144}Nd$ (0.512798) ratios which are less radiogenic than either their host alkali basalt or Damavand basalts, implying significant regional variations in the composition and extent of metasomatism in the sub-Iranian mantle.

1. Introduction

A small isolated outcrop of Neogene, possibly Quaternary, alkali olivine basalt (Fig. 1), containing both peridotite and gabbroic xenoliths, as well as plagioclase megacrysts, was reported on the Kariz-Now geological map (Geologic Survey of Iran, 1984), northeastern Iran. Although this is currently the only known mantle xenolith locality in Iran, there has been no previous petrochemical characterization of either the basalt or these xenoliths. Crustal and mantle xenoliths entrained in continental alkali basalts provide samples to study the chemical and physical evolution of the deep continental lithosphere (Wilson, 1989; Rudnick, 1992; Stern et al., 1999; Farmer, 2003; Gautheron et al., 2005; Nasir et al., 2006). The trace element and isotope signatures of xenoliths and their host basalts can be used to interpret the role of different processes, such as removal of melt by partial melting and/or addition of melt or interaction with fluids, derived from either subducted oceanic lithosphere or asthenospheric upwelling, in the long-term chemical evolution of the lithosphere (Dobosi et al., 2010). This paper presents the petrochemical characteristics of the olivine basalts and their contained xenoliths from northeastern Iran as a contribution toward characterizing the lithosphere below this region, which lies along the Alpine–Himalayan collision belt (Fig. 1).

2. Geologic setting

The oldest rocks in northeastern Iran are Neoproterozoic in age (Fig. 1). These rocks are metamorphic gneisses and schists, recrystallized limestones and dolomites, granites and quartz diorites. The U–Pb in zircon age of one granitic unit is reported as 630–650 Ma (Geologic Survey of Iran, 1984). This crystalline basement is similar to Neoproterozoic to Early Cambrian granites and orthogneisses exposed in other areas of Iran (Hassanzadeh et al., 2008) and to the basement lithologies of the Arabian–Nubian shield.

From Late Precambrian until Late Paleozoic time, central and eastern Iran was separated from the Eurasian plate by the Hercynian Paleotethys Ocean (Shahabpour, 2005). During the Permian–Triassic, a

* Corresponding author at: Department of Geological Sciences, University of Colorado, Boulder, USA.
E-mail address: Saeed.Saadat@Colorado.edu (S. Saadat).

0377-0273/$ – see front matter © 2012 Elsevier B.V. All rights reserved.
doi:10.1016/j.jvolgeores.2012.02.014

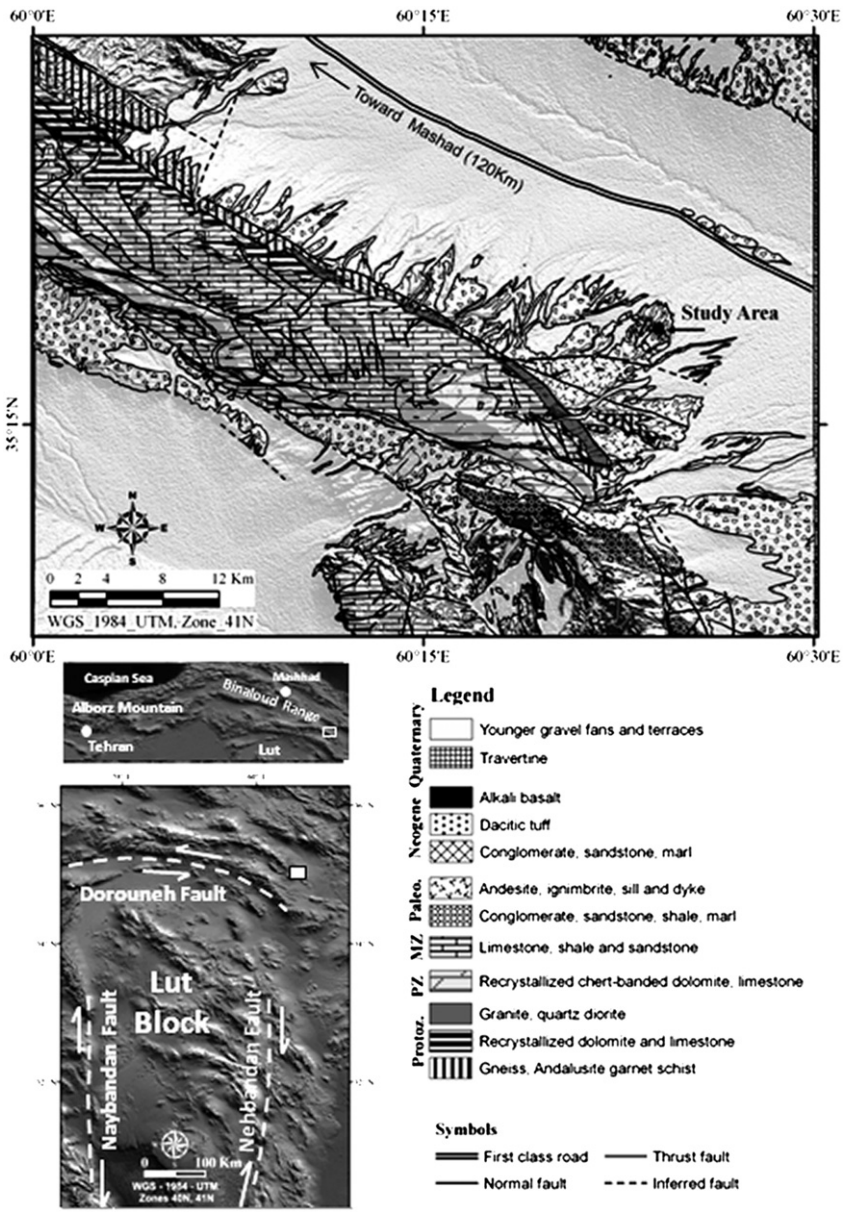

Fig. 1. Simplified geological map of northeastern Iran, Kariz Now area, showing the location of the outcrop of the xenoliths-bearing alkali basalt. The base map is taken from Geologic Survey of Iran (1984). Insets show location of the area in Iran.

north-dipping subduction system along the northern Paleotethys margin led to the closure of this ocean (Golonka, 2004), and the northward motion of central and eastern Iran micro-continent resulted in their welding with the Eurasia. Remnants of the Paleotethys Ocean are present in the Binaloud range in northeastern Iran (Fig. 1; Alavi, 1979). This range extends to the west into the Alborz Mountains and it extends eastward to the Hindu–Kush in northern Afghanistan. The study area is located in the southern portion of the eastern section of Binaloud range in northeastern Iran.

The oldest Paleozoic rocks in this area are composed of sandstone and minor dark gray dolomite that grade upward into a fossiliferous, dark gray limestone of Devonian age (Geologic Survey of Iran, 1984). The sequence of Permian rocks starts with reddish sandstone and follows by a well-bedded dolomitized limestone. Mesozoic rocks in this area mainly consist of bedded limestone, dolomite, shale, sandstone and conglomerate, whereas the Paleogene is marked by volcano-sedimentary rocks. Tertiary volcanic rocks are mostly porphyritic basaltic andesites, dacites, and rhyodacitic welded tuffs (Fig. 1). The latter were dated 38.5 ± 1.2 Ma, indicating a late Eocene–early Oligocene age for the upper part of the volcano-sedimentary sequence (Geologic Survey of Iran, 1984). Neogene sediments, mainly conglomerates and sandstones, form very thick sequences filling in tectonic basins on either side of the main Binaloud range.

The alkali olivine basalt cone which is the focus of this study forms a small isolated outcrop overlying unconsolidated Neogene sediments and Tertiary andesitic and dacitic tuffs (Figs. 1 and 2). This basaltic cone and associated lava flows outcrops in a subcircular area of ~60,000 m^2 (0.3×0.2 km). Relatively extensive layers of Quaternary travertine occur both to the south (Fig. 1) and northwest of this area. These are related to the thermal activities of hot springs, some of which are still active in the area. The presence of host springs with extensive travertine deposits could be regarded as surface expressions of an underlying magma reservoir, or they may simply be related to the structural faults along which the basalt extruded.

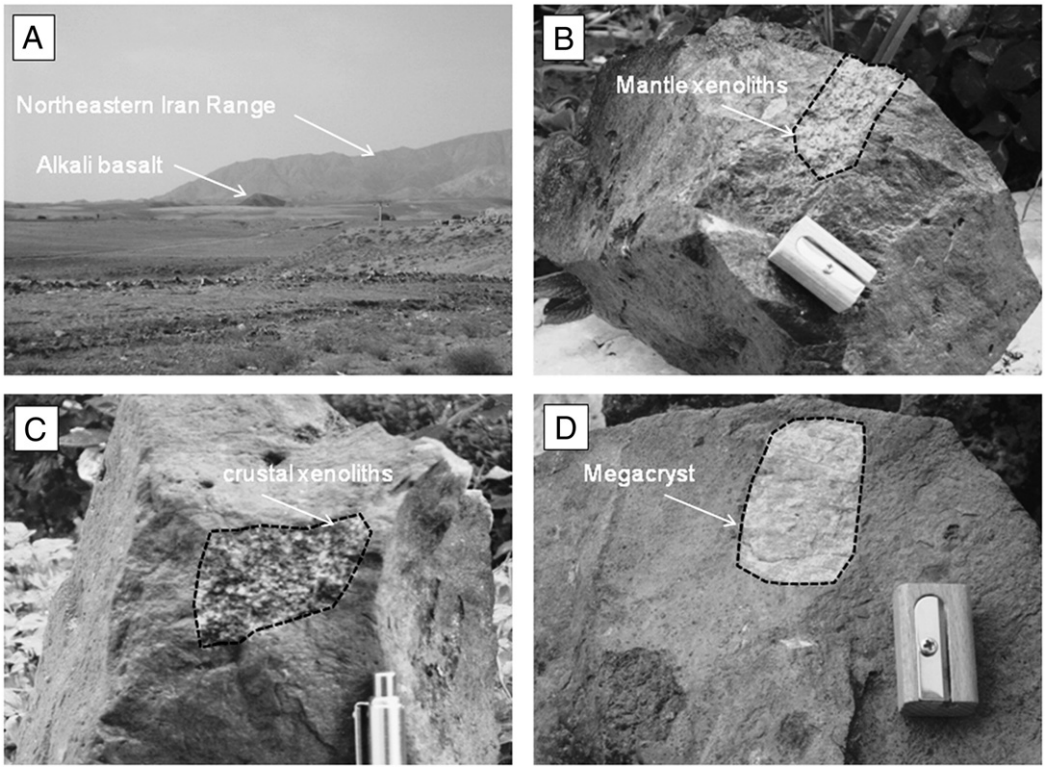

Fig. 2. (A) Field photo of the basaltic cone in northeastern Iran, viewed looking from the highway toward the southeast (Fig. 1), with the mountains in the background; (B) an olivine-rich mantle peridotite xenoliths; (C) a gabbroic crustal xenoliths; and (D) a plagioclase megacryst.

3. Analytical methods

Minerals from the host-rock and xenoliths and were analyzed using a JEOL JXA-8600 electron microprobe, with an electron gun accelerating voltage of 15 kV (10 to 30 s/peak, 5–10 s/background counting times), current range from 17 to 24 nA and 2 μm diameter of focused beam. Matrix correction was done by Tracor Northern ZAF with natural mineral standards. Analytical errors are 0.1–1.0% for major elements. Multiple analyses were done on each mineral grain to check for homogeneity.

Powdered whole-rock samples were analyzed for the major-elements in the X-Ray Fluorescence laboratory of Ferdowsi University of Mashad (Iran), using a Philips X, Unique II instrument. In order to avoid any megacrysts and/or xenoliths, the samples were first crushed into small fragments and then powdered in a ceramic-lined container. Detection limits for Si and Al are 100 and 120 ppm respectively, and for Ca = 55 ppm, Fe = 15 ppm, K = 20 ppm, Mg = 30 ppm, Na = 35 ppm, Mn = 4 ppm and P = 135 ppm. Trace-elements and REE were determined by ICP-MS (Inductively Coupled Plasma Mass Spectrometry) using an ELAN DCR-E instrument at the University of Colorado, Boulder. USGS basalt standards BHVO-1 and NIST2711 were used as the calibration standards and to monitor accuracy during ICP-MS analysis. Precision for analytical technique is generally better than 10% at the 95% confidence level as indicated by repeat analysis of these and another laboratory basalt standard VDM derived from Valmont dike in Boulder (Saadat and Stern, 2011).

The facilities of the Tims isotope laboratory in the University of Colorado-Boulder were used for sample preparation and isotope analyses. Isotopic measurements were carried out on powder of leached whole-rock material using a Finnigan-Mat 261 six collector thermal-ionization mass-spectrometer. In addition, pyroxenes from peridotite xenoliths and a plagioclase megacryst were analyzed for isotopic composition. Separation of the xenoliths pyroxenes was done by hand picking grains. Sample powders were generated in a ceramic-lined container. $^{87}Sr/^{86}Sr$ ratios were analyzed using four-collector static mass spectrometer. Replicate analyses of the SRM-987 standard in this mode yielded a mean $^{87}Sr/^{86}Sr$ of 0.71025 ± 2 (2σ). Measured $^{87}Sr/^{86}Sr$ were corrected to SRM-987 = 0.710299 ± 8. Errors are 2σ of mean and refer to last two digits of the $^{87}Sr/^{86}Sr$ ratio. The Nd isotopic compositions are reported as ε_{Nd} values using a reference $^{143}Nd/^{144}Nd$ ratio of 0.512638. Measured $^{143}Nd/^{144}Nd$ were normalized to $^{146}Nd/^{144}Nd = 0.7219$. Analyses were dynamic mode, three-collector measurements. Thirty-three measurements of the La Jolla Nd standard during the study period yielded a mean $^{143}Nd/^{144}Nd = 0.511843 \pm 8$ (2σ mean). Details of analytical procedures are given in Farmer et al. (1991, 2002). Pb isotopic analyses were four-collector static mode measurements. Sixteen measurements of SRM-981 during the study period yielded $^{208}Pb/^{204}Pb = 36.56 \pm 0.03$, $^{207}Pb/^{204}Pb = 15.449 \pm 0.008$, $^{206}Pb/^{204}Pb = 16.905 \pm 0.007$ (2σ mean). Measured Pb isotope ratios were corrected to SRM-981 values of $^{208}Pb/^{204}Pb = 36.721$, $^{207}Pb/^{204}Pb = 15.491$, $^{206}Pb/^{204}Pb = 16.937$. Total procedural blanks averaged ~1 ng for Pb and Sr, and 100 pg for Nd during study period (Farmer et al., 2002). No age correction was applied to the data because of the young Neogene age of the rocks.

4. Results

4.1. Basalts

4.1.1. Petrography and mineral chemistry

Different samples from the cone and associated lavas have similar porphyritic texture with up to 10% phenocrysts and micro-phenocryst within intergranular to intersertal groundmass (Fig. 3A). No significant textural differences were observed among different samples, suggesting that this cone was formed in a single monogenetic event. Subhedral olivines are the most common phenocrysts. Plagioclase is also observed as a phenocryst, but clinopyroxene is rare. The groundmass is mostly composed of microlites of plagioclase, clinopyroxene, olivine and minor sanadine. In addition opaque oxides, mainly titano-magnetite, along with apatite and a small volume of glass are present in the

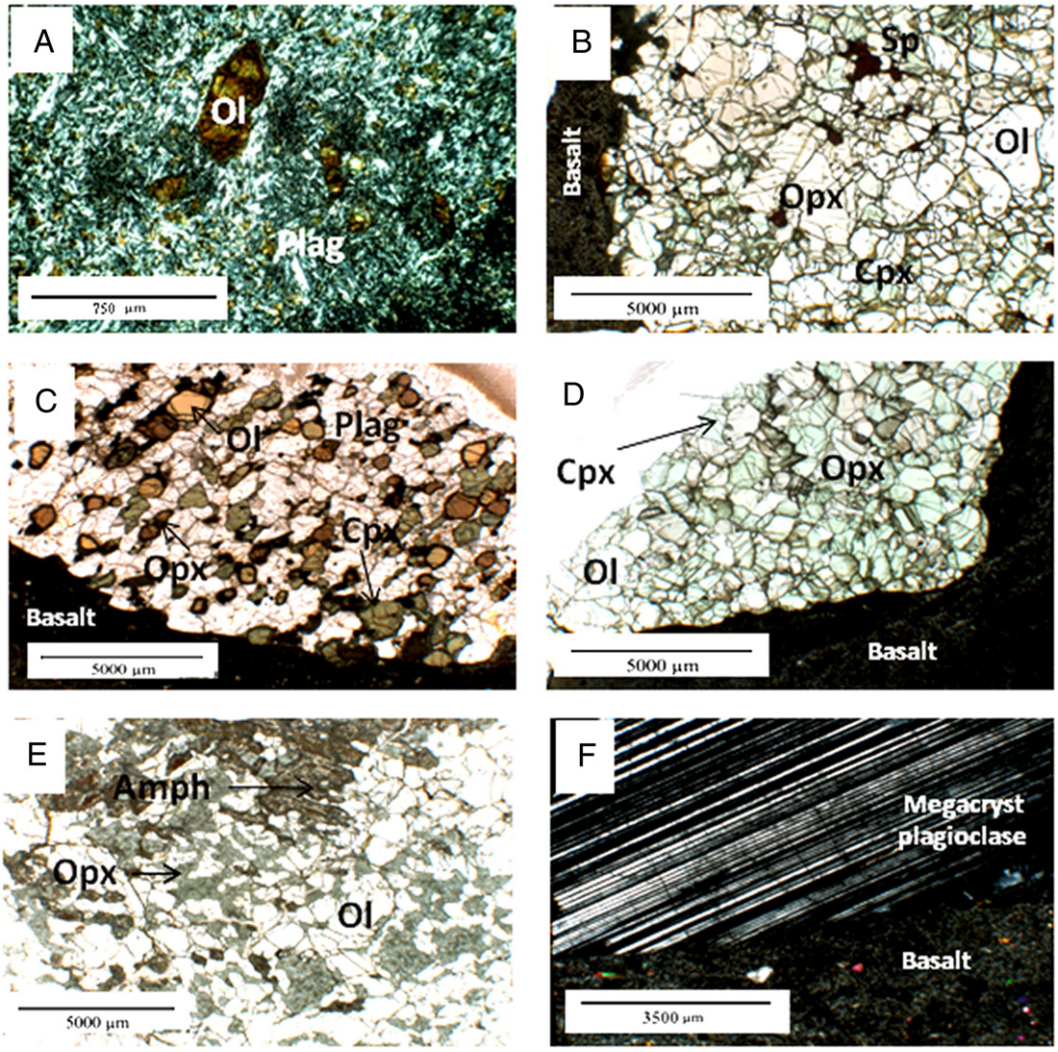

Fig. 3. Photomicrographs of (A) alkali basalt, (B) spinel lherzolite, (C) gabbroic xenoliths, (D) pyroxenite, (E) lherzolite with amphibole, and (F) plagioclase megacryst.

groundmass. Both phenocrysts and groundmass show little evidences of alteration, but calcite occurs as a secondary mineral filling vehicles and fractures.

Mantle peridotite and deep-crustal meta-igneous granulite xenoliths, as well as megacrysts of plagioclase, all described in greater detail below, are present in the basalt (Fig. 2). Xenocrysts of olivine and pyroxene, derived from fragmented peridotite xenoliths, are also observed in thin sections. They are distinguished from phenocrysts by their relatively large size, occurrence as composite grains, and Mg-rich compositions compared to phenocryst and groundmass minerals crystallized from the basalt host (Fig. 4). No quartz xenocrysts or other visual evidence of assimilation of upper crustal rocks was observed in the basalts.

Olivine phenocrysts in the basalt range in composition from Fo_{72} to Fo_{83} and their NiO contents range between 0.06 and 0.14 wt.% (Table 1; Fig. 4). There is no significant variation between cores and rims of olivine. The chemistry of two clinopyroxene phenocrysts, which are rare, is high-Ti augite. Plagioclase in the alkali basalt has composition ranging from $An_{28\text{-}59}$.

4.1.2. Whole rock chemistry

The major and trace element concentrations of five separate samples of the basalt, as well as their average and the average composition of the other Neogene alkali olivine basalts from the western Lut block in east-central Iran and the Makran arc in southern Iran, are listed in Tables 2 and 3. All samples of the olivine basalt from northeastern Iran plot in the alkalic field on a silica versus total alkalis classification diagram (Fig. 5). Normative nepheline of the samples varies from 7 to 11% confirming the alkalinity of these basalts. These lavas also plot in the alkali basalt field, or very close to the boundary of alkali basalt and foidite fields, on a Nb/Y versus Zr/Ti diagram (Fig. 5). The K_2O/Na_2O ratio and MgO versus TiO_2 diagrams show that these lavas plot on the boundary of high- and low-Ti fields and they belong to Na-Series alkali basalts (Fig. 5). The samples have moderate MgO (4.1–7.4 wt.%) and Al_2O_3 (16.2–18.4 wt.%) contents and their Cr and Ni concentrations range from 52 to 84 ppm and from 86 to 109 ppm, respectively.

Chondrite-normalized patterns of northeastern Iran alkali basalt (Fig. 6) indicate that these lavas are enriched in LREE relative to HREE and are similar to that of average oceanic island basalts (OIB; Sun and McDonough, 1989). There is no significant difference between the trace and rare element patterns of these samples and those of samples from the western margin of the Lut block along the Nayband fault (Table 3, Fig. 6). None of the samples show depletions in Nb, which is a signature for subducted slab-derived components in the source of arc magmas such as those in the Makran arc in southern Iran. Neither do Sr nor Eu shows a negative anomaly, which suggests that they behaved incompatibly for these lavas (Fig. 6).

Rb contents, as well as K_2O and Sr, are somewhat variable among the five different samples (Fig. 6). These variations in mafic magmas could be caused by several different processes such as wall-rock reaction (Green and Ringwood, 1967), variable degrees of partial melting (Gast, 1968) and mantle heterogeneity (Kesson, 1973). However, since these variations occur within what appears to be a single small

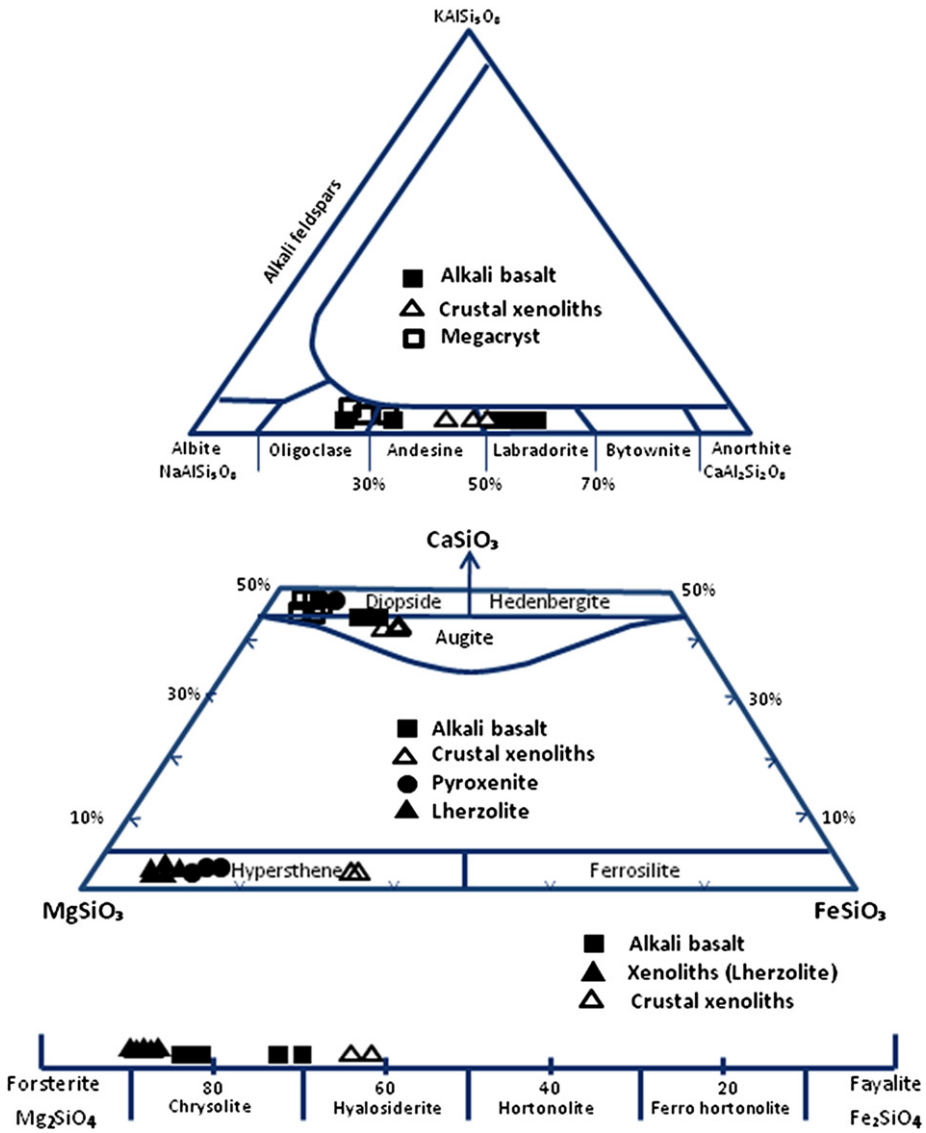

Fig. 4. Compositions of olivines, orthopyroxenes, clinopyroxenes and plagioclases in the alkali basalts (solid square), spinel–lherzolite xenoliths (solid triangles), pyroxenite xenoliths (solid circle), meta-gabbroic crustal xenoliths (open square), and plagioclase megacrysts (open square).

monogenetic cone and associated lava flows, and since the variation for most all other elements is small (Fig. 6, Tables 2 and 3), they might result simply by migration of late stage magmatic liquids (Hart et al., 1971).

4.1.3. Radiogenic isotopes

Sr–Nd–Pb isotopic ratios for the Neogene alkali olivine basalts are given in Table 4. Their isotopic characteristics are compared with the other Neogene/Quaternary alkali basalts from the western Lut block, Makran arc, and also Quaternary basaltic samples from north-central and northwest Iran (Fig. 7). The measured $^{87}Sr/^{86}Sr$ ratios from two samples of this basalt are 0.705252 and 0.705013 and the $^{143}Nd/^{144}Nd$ isotopic compositions are 0.512738 and 0.512735. The Pb isotopic composition of these alkali basalts plots above the Northern Hemispheric Reference Line (NHRL), in the EM-2 of OIB (Fig. 8).

4.2. Ultramafic mantle xenoliths

4.2.1. Petrography

Ultramafic xenoliths found in this study are Group I peridotites (Lloyd and Bailey, 1975; Frey and Prinz, 1978; Lloyd, 1987), including spinel lherzolites, harzburgites, wehrlites and pyroxenites all containing emerald green Cr-diopside clinopyroxenes. These xenoliths, which are only as large as 7 cm across, are fractured, but do not show any sign to indicate shearing or other ductile deformation, and they have coarse granular textures with 120° triple junctions between crystal grain boundaries indicating a static recrystallization process (Fig. 3; Pearson et al., 2003). Some xenoliths exhibit decompression melt textures along mineral grain boundaries. Weathering and/or serpentinization are either minimal or absent in most xenoliths.

The spinel lherzolith xenoliths are composed of about 50–60 modal % olivine, 25–35% orthopyroxene, 20–25% clinopyroxene, and 1–5% Cr-spinel. Olivine abundances are 80–90 modal % in a few samples, which places them near the dunite–harzburgite boundary. Wehrlite and pyroxenite xenoliths are composed of 10–15% olivine, 50–60% orthopyroxene, 30–35% clinopyroxene and minor spinel (Fig. 3). In one lherzolite xenolith (NXP-4), a few grains of brown amphibole (<5%) are present. In addition titanomagnetite, magnetite, ilmenite, and copper sulfides are present. There is a spongy texture in some clinopyroxene grains, reflecting incipient melting.

4.2.2. Mineral chemistry

Olivines in lherzolites are very homogenous with high magnesium content (Fo_{88-90}; Fig. 4; Table 5). NiO in olivine ranges from 0.32 to

Table 1
Compositions of representative olivine, clinopyroxene and plagioclase in the host basalt.

Mineral	Clinopyroxene		Plagioclase				Olivine		
Sample	NXP 11-2		NXM 2	NXM 2	NXG		NXP 10	NXM 5	NXP 11-1
No.	2		1	2	4		1	3	3
SiO_2	49.3	SiO_2	53.3	60.9	53.8	SiO_2	38.5	38.8	40.0
TiO_2	1.9	Al_2O_3	29.5	24.3	29.1	FeO	24.8	24.3	16.4
Al_2O_3	4.1	FeO	0.6	0.6	0.8	MnO	0.7	0.6	0.2
Cr_2O_3	0.01	CaO	11.3	5.7	10.9	NiO	0.1	0.1	0.1
FeO	9.2	Na_2O	4.5	6.8	4.7	MgO	36.7	36.8	44.1
MnO	0.2	K_2O	0.4	0.7	0.2	Total	100.8	100.6	100.8
MgO	13.3	Total	99.5	99.3	99.6				
CaO	21.4					*Cations calculated on the basis of 4 oxygens*			
Na_2O	0.6	*Cations calculated on the basis of 32 oxygens*							
Total	100.2					Fe	0.54	0.53	0.34
		Si	9.71	11.02	9.80	Mn	0.02	0.01	0.01
Cations calculated on the basis of 6 oxygens		Al	6.32	5.19	6.24	Ni	0.02	0.01	0.01
		Fe	0.09	0.09	0.12	Mg	1.40	1.43	1.63
Si	1.84	Ca	2.20	1.10	2.12				
Al	0.19	Na	1.60	2.37	1.67	Fo	72	72	83
Ti	0.05	K	0.09	0.24	0.06				
Cr	0.00								
Fe	0.29	Or	2	7	1				
Mn	0.01	Ab	41	63	44				
Mg	0.74	An	57	30	55				
Ca	0.86								
Na	0.05								
En	40								
Wo	45								
Fs	15								
Mg#	76								

0.44 wt.%. The Mg# of both lherzolite and pyroxenite clinopyroxenes are similar or slightly greater than that of coexisting olivine, ranging from 88 to 93 (Tables 6a and 6b). These clinopyroxenes are all emerald green Cr-diopsides with a limited range of composition of $Wo_{45-46}En_{47-50}Fs_{4-7}$ (Fig. 4). Al_2O_3 in lherzolite clinopyroxene ranges from 5.2 to 7.2 wt.% and Cr_2O_5 ranges from 0.4 to 1.0 wt.% (Table 6a), while in pyroxenite clinopyroxenes Al_2O_3 (1.7 to 2.6 wt.%) and TiO_2 are lower (Table 6b), but Cr_2O_5 contents are similar to clinopyroxenes in lherzolites. Lherzolite orthopyroxenes show a very small range in composition ranging from $En_{88-90}Fs_{9-10}Wo_{1-2}$ with Mg# = 91–92 (Fig. 4) similar to that of clinopyroxenes (Table 7a). The Al_2O_3 content of lherzolite orthopyroxenes varies between 3.6 and 4.8 wt.% and their CaO contents range from 0.7 to 0.8 wt.% (Table 7b). Orthopyroxenes in pyroxenites have lower Mg# (86–90; Fig. 4) and Al_2O_3 contents (1.4 to 2.1 wt.%; Table 7b), as well as higher FeO compared to lherzolite orthopyroxenes. There is either only a very small or no detectable variations in the elements Mg, Fe, Ca, and Al from core to rim in either pyroxenes. The trace-element composition of one clinopyroxene separated from a pyroxenite xenolith is presented in Table 8.

Amphibole occurs in just one sample (NXP-4, Table 9). Based on their equigranular textures these amphiboles were stable in the mantle, but they show reaction edges due to decompression melting.

Table 2
Major element concentrations (in oxide wt.%) of the basalts in northeastern Iran (NEI) compared with the average of Neogene/Quaternary basalts from western Lut block (WLUT) and Makran arc (MAK).

Sample	N1	N2	N3	N4	N5	Ave. NEI	Ave. WLUT	Ave. MAK
No.						5	8	9
SiO	49.5	49.4	48.8	48.4	50.6	49.3	49.1	48.4
TiO	1.9	1.9	2.2	2.1	2.0	2.0	2.5	1.0
Al O_3	16.9	17.3	16.2	18.4	17.4	17.2	14.3	17.5
FeO	10.4	10.5	10.9	11.6	10.5	10.8	11.2	8.6
MnO	0.2	0.2	0.2	0.2	0.2	0.2	0.2	0.1
MgO	4.4	5.0	7.4	4.1	4.7	5.1	5.8	6.4
CaO	5.9	5.4	5.9	5.9	5.6	5.7	8.3	10.9
Na O	5.8	5.5	4.9	5.1	5.4	5.3	4.6	3.8
K O	2.2	2.5	1.7	2.6	2.1	2.2	1.8	0.8
P O_5	0.4	0.3	0.4	0.4	0.4	0.4	0.5	0.2
Total	97.6	98	98.6	98.8	98.9	98.2	98.1	97.6
K O + Na O	8.0	8.0	6.6	7.7	7.4	7.6	6.4	4.6
K O/Na O	0.4	0.5	0.4	0.5	0.4	0.4	0.4	0.2
Norm. neph.	11.5	11.0	7.2	10.9	6.7	9.5	3.6	6.1

Major element data are from XRF analysis. Mg# = 100 Mg/(Mg + Fe^{+2}) calculated with Fe^{2+} = 0.85 (total Fe). Total Fe reported as FeO. Norm. neph. = Norrmative nepheline. N = northeastern Iran basalts, WLUT = western Lut Neogene/Quaternary basalts along the north and middle part of the Nayband fault from Saadat et al. (2010), MAK = Quaternary basalt from the Makran arc from Saadat and Stern (2011).

Table 3
Trace element concentrations (in ppm) of Neogene and Quaternary basalts from eastern Iran.

Sample	N1	N2	N3	N4	N5	Ave. NEI	Ave. WLUT	Ave. MAK
No.						5	8	9
Ni	86	102	98	109	89	97	131	107
Cr	69	74	53	84	52	66	189	149
V	155	161	171	178	159	165	187	222
Cs	1.5	1.6	1.5	1.7	1.5	1.6	0.6	0.8
Rb	22	31	99	14	50	43	37	22
Ba	481	580	630	588	611	578	405	229
Sr	573	587	750	717	777	681	938	669
Nb	43	46	47	45	49	46	52	9
Ta	3.3	3.2	3.5	2.6	3.2	3.2	5.0	2.0
Zr	214	216	213	202	227	214	196	117
Ti	10,359	10,629	11,483	11,369	10,960	10,960	14,642	6646
Y	14	18	19	18	18	17	20	18
Hf	4.9	5.2	5.0	4.8	5.4	5.1	4.5	3.0
Th	3.0	3.2	3.2	3.2	3.4	3.2	3.6	2.7
U	2.1	0.8	0.7	0.8	0.8	1.0	0.9	0.7
La	19.8	22.0	22.4	21.2	23.6	21.8	31	14
Ce	42.0	44.5	46.6	44.5	48.6	45.3	62.0	30.8
Pr	4.95	5.27	5.60	8.10	5.79	5.94	6.96	3.59
Nd	21.3	23.0	24.8	25.4	25.4	24.0	30.27	15.61
Sm	5.03	5.00	5.60	5.35	5.65	5.33	6.55	3.13
Eu	1.59	1.68	1.98	1.84	1.78	1.77	2.09	1.07
Gd	5.18	5.74	5.95	6.03	6.17	5.81	7.36	3.94
Tb	0.60	0.67	0.78	0.78	0.76	0.72	0.88	0.56
Yb	1.27	1.30	1.34	1.41	1.46	1.35	1.44	1.69
Lu	0.16	0.15	0.19	0.17	0.19	0.17	0.20	0.29
Zr/Nb	5.0	4.7	4.5	4.5	4.6	4.6	4.6	14.9
La/Nb	0.46	0.47	0.47	0.47	0.48	0.47	0.59	1.77
Ba/Nb	11.2	12.5	13.3	13.1	12.4	12.5	8.7	26.9
La/Yb	15.6	16.9	16.7	15.1	16.2	16.1	20.8	8.2
Ba/Zr	2.2	2.7	3.0	2.9	2.7	2.7	2.1	2.0
$(La/Yb)_N$	10.1	11.2	11.4	10.0	10.4	10.6	13.7	5.9

4.2.3. Radiogenic isotopes

For clinopyroxenes separated from two different pyroxenite xenoliths the $^{87}Sr/^{86}Sr$ ratios are 0.704593 and 0.704309, and the $^{143}Nd/^{144}Nd$ ratio for the first one is 0.512798, values which differ from the host basalt (Fig. 7; Table 4).

4.2.4. Thermometry

The compositions of two adjacent pyroxene grains in xenoliths were used for thermometry according to Brey and Kohler (1990). We calculated a very similar and limited range of temperatures, between 990–1030 °C for pyroxenite and 990–1044 °C for lherzolite xenoliths (Fig. 9; Table 10), assuming an equilibrium pressure of 1.5 GPa appropriate for spinel lherzolites. Because of the homogeneity of these minerals, there is no significant difference in estimated temperature between their core and rim, but different pyroxene pairs within one sample sometimes record small temperature differences (±20 °C) which may be related to analytical error.

4.3. Gabbroic xenoliths

4.3.1. Petrography

Rounder to angular gabbroic xenoliths, ranging from ~1 to 6 cm in longest dimension, are composed of ~50% plagioclase as well as both clinopyroxene and orthopyroxene and small amounts of olivine (<5%). These have granoblastic textures (Figs. 2 and 3). Olivines have undergone reactions with plagioclase to produce fine grained symplectic intergrowths of minerals (mainly pyroxene). Some plagioclases also show spongy texture that could be the result of dissolution and/or direct melting caused by heating within the hotter mafic host magma which transported the xenoliths to the surface (Hibbard, 1995). Apatite and titanomagnetite are also present in these lower crustal xenoliths.

4.3.2. Mineral chemistry

The composition of the plagioclases ranges from An_{44-51} (Fig. 4; Table 11). The clinopyroxenes have a limited range of composition ($Wo_{37-43}En_{38-45}Fs_{18-19}$; Fig. 4), with Mg# between 70 and 75. Orthopyroxene shows a constant composition as $En_{62}Fs_{36}Wo_2$ and Mg# = 67 (Fig. 4) and olivines are Fo_{62-64} (Fig. 4).

4.4. Plagioclase megacrysts

Plagioclase megacrysts, with maximum length of 4 cm, have sharp euhedral crystal faces and there is no evidence of reaction between the edge of these minerals and host rocks (Figs. 2 and 3). Megacryst plagioclase has composition ranging from An_{26-32} (Fig. 4; Table 11) and no zoning was observed in thin section and microprobe analyses. The potassium contents for plagioclase megacryst are higher (7–10%) than that of plagioclase of basalts (1–8%). The $^{87}Sr/^{86}Sr$ ratio for a plagioclase megacryst is somewhat lower (0.704796) than that of the host basalts and its $^{143}Nd/^{144}Nd$ ratio is 0.512687 (Table 4, Fig. 8).

5. Discussion and conclusions

5.1. Generation of the alkali basalts

The small volume of Neogene basaltic lavas which have erupted in the northeastern Iran indicates within-plate alkali basalt characteristics. Generation of this type of magma is generally considered consistent with an extensional tectonic regime (e.g., Wilson, 1989). An early to mid-Tertiary extensional tectonic regime occurred in central and northern Iran (Brunet et al., 2003; Hassanzadeh et al., 2004) resulting in the development of Cordilleran-style metamorphic core complexes (Kargaran et al., 2006; Moritz et al., 2006; Verdel, 2009). However, the final closure of Neotethys and collision between Arabia and central-

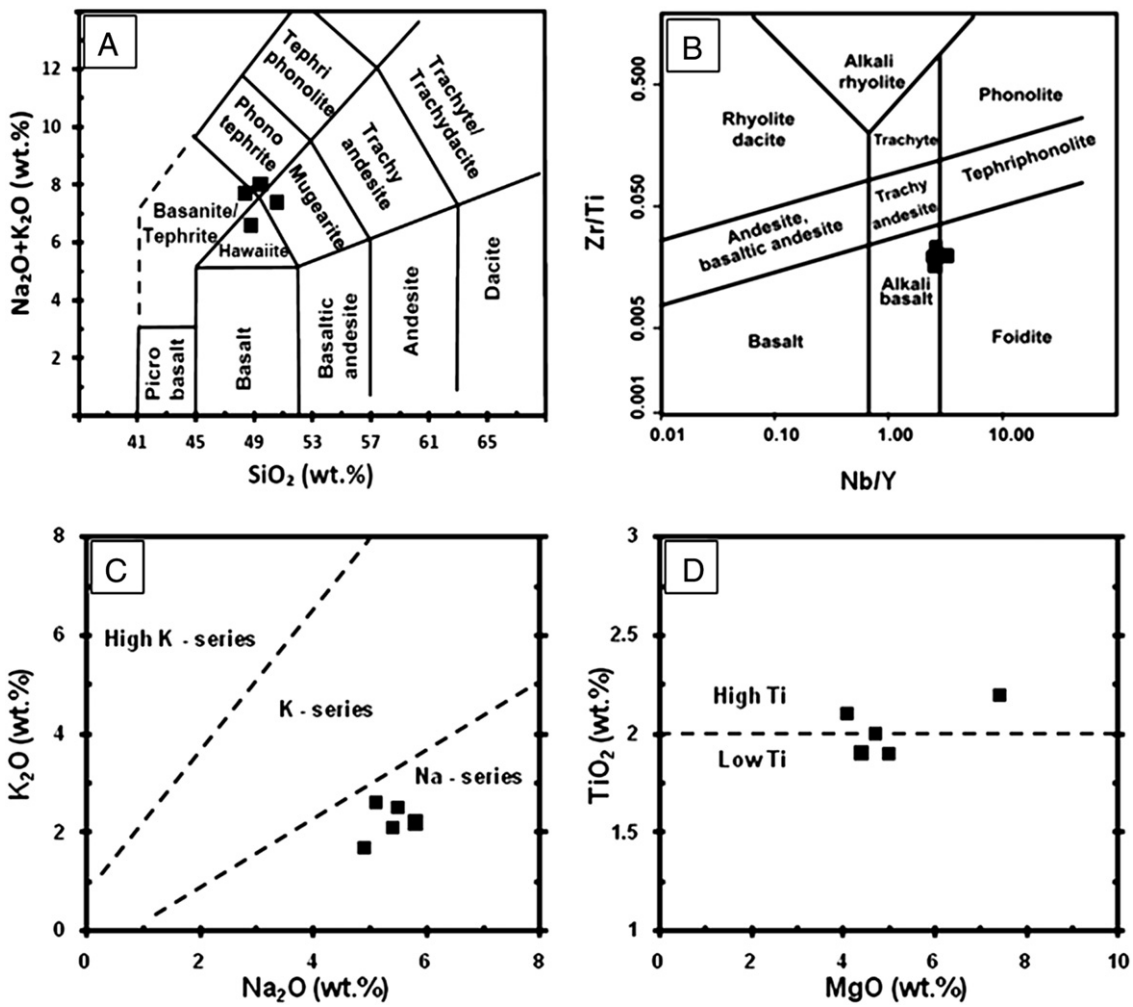

Fig. 5. (A) Geochemical division (Le Maitre et al., 2002) of 5 separate samples of the alkali basalt based on $Na_2O + K_2O$ (wt.%) against SiO_2 (wt.%). (B) Zr/Ti versus Nb/Y diagram modified from Pearce (1996) showing that all samples plot in the field of alkali basalt. (C) K_2O versus Na_2O diagram, showing the samples belong to the Na-series after Middlemost (1975), and (D) TiO_2 versus MgO indicates that the content of Ti is relatively high in these alkali basalts.

eastern Iran in the late Oligocene to early Miocene (Fakhari et al., 2008; Horton et al., 2008) led to a transition from an extensional to a contractional tectonic regime as Arabia collided with Eurasia, and the main tectonic features of eastern Iran, at least since ~25 Ma, were created by compression (Fakhari et al., 2008; Horton et al., 2008). The timing of subduction related to plate collision, the role of the trench pulling force and the movement velocity varied for different plates. These differences led to the development of several major strike-slip faults, which cut the continental crust (Jackson, 1992; Kopp, 1997; Golonka, 2000). Eastern Iran is dominated by two belts of N–S right-lateral strike-slip faulting which border the Lut block (Fig. 1); the eastern Nehbandan–Sistan fault system and western Nayband–Gowk system. Both of these long strike-slip faults also exhibit components of shortening and reverse faulting. These belts accommodate N–S right-lateral shear and some shortening between eastern Iran and western

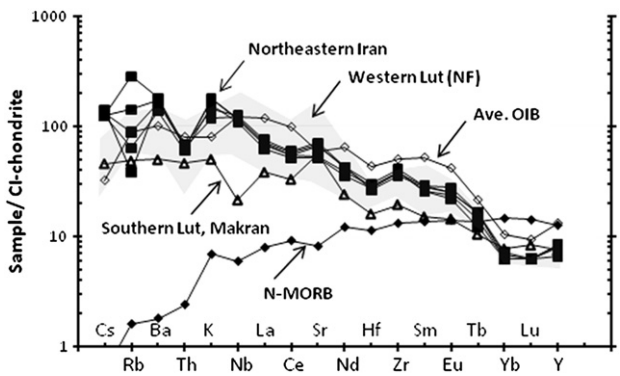

Fig. 6. Chondrite normalized multi-element spider diagram for northeastern Iran Neogene alkali basalt samples and also for western Lut block and Makran arc Neogene basalts. For comparison, average OIB and MORB are added to this diagram. Normalization chondrite values are from Sun and McDonough (1989), average OIB from Sun (1980), MORB (N-type) from Sun (1980) and Saunders and Tarney (1984), average western Lut block from Saadat et al. (2010), and Makran arc from Saadat and Stern (2011).

Table 4
Sr, Nd, and Pb isotopic compositions of northeastern Iran basalt, clinopyroxene from mantle peridotite xenoliths and a plagioclase megacryst.

Sample	$^{87}Sr/^{86}Sr$	$^{143}Nd/^{144}Nd$	ε_{Nd}	$^{206}Pb/^{204}Pb$	$^{207}Pb/^{204}Pb$	$^{208}Pb/^{204}Pb$
NE Iran						
N1	0.705250	0.512738	+2.0	18.53	15.54	38.44
N3	0.705013	0.512735	+1.9	18.44	15.53	38.13
Na (CPX)	0.704309					
Nb (CPX)	0.704593	0.512798	+3.1			
Plag. megacryst	0.704796	0.512687	+1.0	18.25	15.48	38.16

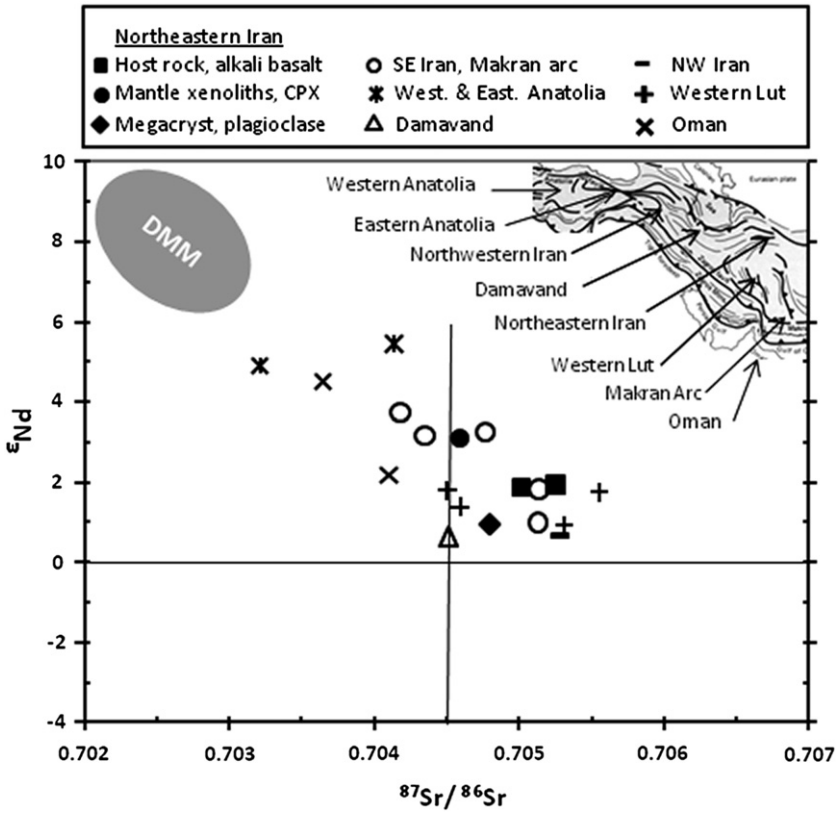

Fig. 7. $^{87}Sr/^{86}Sr$ ratio versus ε_{Nd} comparing northeastern Iran samples (Table 4) with the other alkali basalts around the Lut block, north and northwestern Iran, western Anatolia (Alicic et al., 2002; Kheirkhah et al., 2009), Eastern Anatolia (Pearce et al., 1990) and Oman (Nasir et al., 2006).

Afghanistan (Ambraseys and Bilham, 2003). North of ~34°N, right lateral shear is achieved on left lateral faults that are thought to generate clockwise rotation in the Lut block (Fig. 1). The extent of rotation has increased from west to east during last ~5 Ma (Jackson and McKenzie, 1984; Walker and Jackson, 2004; Walker et al., 2004). This structural feature might be suitable to develop an episode of localized extension-induced fractures at the projected junction between the N–S right-lateral and E–W left-lateral strike slip fault in this area, which is close to where the xenoliths-bearing alkali basalt outcrop occurs in northeast Iran. The occurrence of such localized tensional forces might act as an open space through which basaltic magma could reach the surface. Tomographic imaging of the uppermost mantle velocity in this area shows relatively low P_n velocity (Al-Lazki et al., 2004; Tabatabai Mir et al., 2008), implying the presence of an anomalously hot and/or thin mantle lid. Thus, the monogenetic basalt cone that is the focus of this study is not unexpected, and other larger outcrops of alkali olivine basalts occur both within and along both the eastern and western boundaries of the Lut block (Saadat et al., 2010).

5.2. Nature of their mantle source region

The alkali basalt from northeastern Iran has OIB-like intra-plate geochemical characteristics. In these samples Nb and Ta are not depleted relative to the LILE (Rb and Ba; Fig. 6) and the ratio of incompatible trace elements such as Ba/Nb (11.2–13.3) and La/Nb (0.5) is similar to some oceanic island basalts (Fig. 10). The measured $^{87}Sr/^{86}Sr$ and $^{143}Nd/^{144}Nd$ ratios plot in the OIB field, similar to those reported by Saadat et al. (2010) from alkali basalts erupted along the Nayband fault west of the Lut block (Fig. 7). Lead-isotopic compositions of all these basalts also overlap the EM-2 and OIBs field (Fig. 8).

Based on a HREE concentration that is ~6× chondritic abundance (Fig. 6) and the high $(La/Yb)_N$ value (10–11) and low Lu/Hf (<0.04), the primary basaltic magma can be attributed to melting in the presence of residual garnet and therefore at least some portion of the melting must have occurred at depth below the spinel to garnet transition in mantle peridotite (e.g., Frey et al., 1978; Langmuir et al., 1992; Thirlwall et al., 1994; Beard and Johnson, 1997; Farmer, 2003). A plot of Zr/Nb versus Ce/Y ratios (Fig. 11), however, suggests that the basalts could have been produced by variable degrees of partial melting process from either the spinel or garnet facies. Fractional crystallization of olivine, clinopyroxene and plagioclase can only generate small changes in these ratios. For example, even 50% fractionation of cpx from an intra-plate magma with Zr/Nb = 10 would only lower Zr/Nb to 9.1 (Thirlwall et al., 1994). Other processes such as crustal contamination also would not produce the composition of these basalts (Fig. 11). Continental crust generally has Zr/Nb >10 and high Ce/Y ratios (e.g., Taylor and McLennan, 1985). Zr/Nb and Ce/Y ratios of samples from northeastern Iran vary from 4.5 to 5 and 2.5 to 3 respectively, suggesting that crustal contamination was limited, consistent with the rapid rise of the basaltic magma through the crust required to bring the relatively dense peridotite xenoliths to the surface, and that instead a combination of melting from both garnet-facies and spinel-facies mantle may be involved in producing these basalts (Fig. 11).

Other element ratios useful for constraining melting models are LREE/HREE ratios versus HREE contents, e.g. La/Yb versus Yb (Baker et al., 1997). These together can distinguish between melting the spinel and garnet fields (Thirlwall et al., 1994; Baker et al., 1997), because there is a very small change in La/Yb ratio in spinel-facies melting compared with their mantle source (Fig. 11), while in contrast, there are large changes in Yb associated with melting in the garnet-facies (Baker et al., 1997). Based on the La/Yb versus Yb of alkali basalts

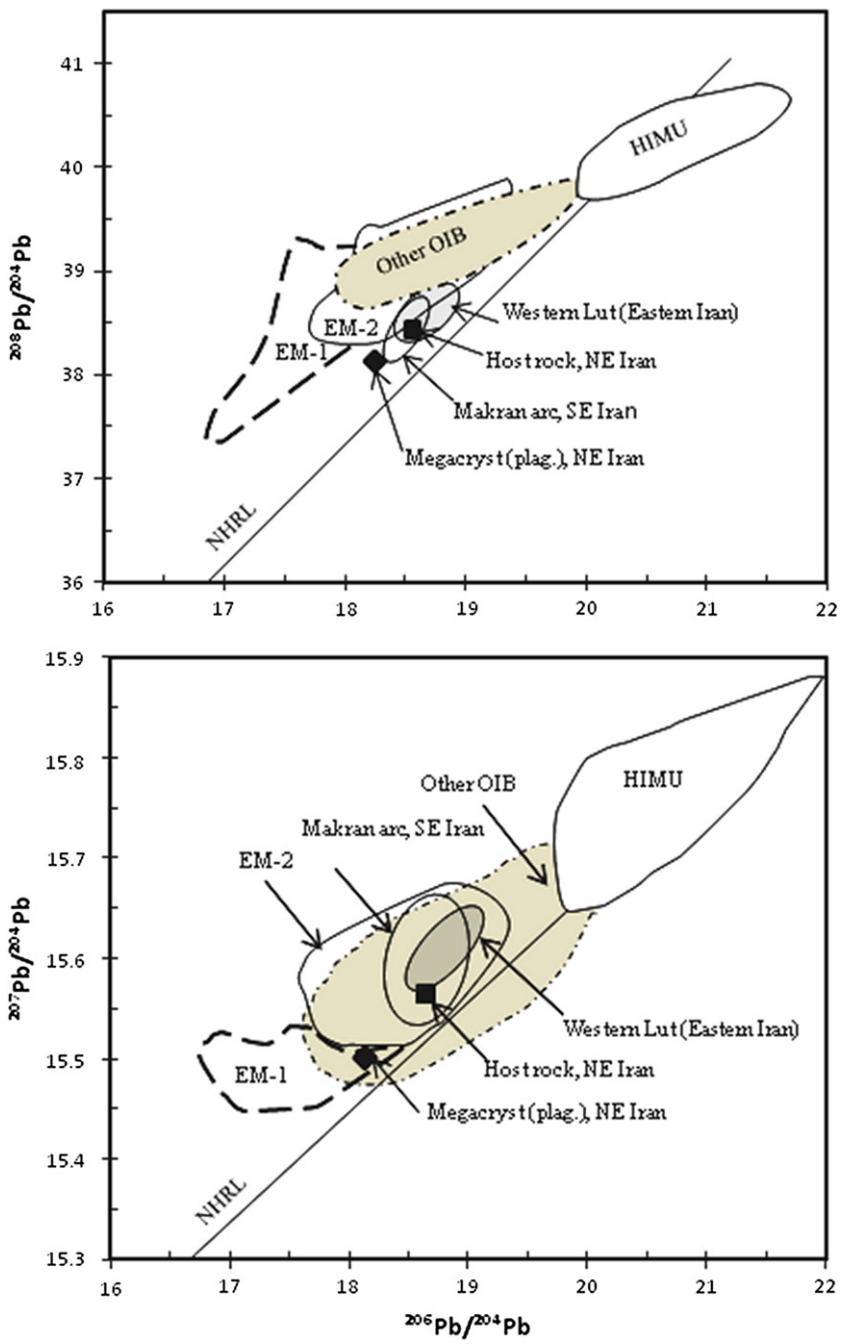

Fig. 8. Plot of $^{207}Pb/^{204}Pb$ and $^{208}Pb/^{204}Pb$ versus $^{206}Pb/^{204}Pb$. Base diagram from Hofmann (1997) and references therein. Source of data similar to Fig. 7. NHRL = Northern Hemisphere Reference Line from Hart (1984).

from northeastern Iran, neither variable degrees of partial melting of a spinel lherzolite nor garnet lherzolite alone can generate the observed La/Yb ratio with Yb contents of these basalts (Fig. 11). Another possible model for the REE composition of the northeast Iran alkali basalts involves mixing of small melt fraction from garnet-facies mantle with relatively larger melt fractions from spinel-facies mantle (Fig. 11). This model is similar to that proposed by Baker et al. (1997) in which the Quaternary intraplate volcanic rocks from western Yemen result from mixing of melts from both spinel and garnet lherzolite facies.

Some experimental evidences demonstrate that SiO_2 content of primary tholeiitic to alkali basaltic melts mainly reflects the pressure of melt formation. Decreasing pressure leads to increasing SiO_2 in the melt (e.g., Hirose and Kushiro, 1993; Walter, 1998). The northeastern Iran alkali basalts have 48–50 wt.% SiO_2 and these values correspond to pressures of 13.2 to 21.9 kbars and depths of 71–45 km based on pressure calculations using the equation $P_{GPa} = 23.217 - 0.4381SiO_2$ with a correlation factor R = 0.878 (Haase, 1996), and pressure-depth conversion made using the relationship $depth_{km} = 3.02\ P_{kbar} + 5$ (Scarrow and Cox, 1995). This estimation of pressure is consistent with the maximum pressure of the garnet-free mantle xenoliths (~19 kbars; see discussion below) and suggests that the basalts from northeastern Iran could be derived from a depth close to the transition between garnet and spinel-facies mantle and consistent with the involvement of both in the generation of these basalts.

Table 5
Compositions of olivine in peridotite xenoliths.

Lithotype	Lherzolith				
Sample	NXP 1	NXP 4	NXP 10	NXP 11-2	NXP 5
No.	3	3	3	3	3
SiO_2	40.8	40.3	41.1	41.8	41.4
FeO	10.8	11.6	10.2	10.3	10.3
MnO	0.2	0.2	0.2	0.2	0.2
NiO	0.4	0.3	0.4	0.4	0.4
MgO	48.3	48.5	49.3	48.2	48.3
Total	100.8	101.0	101.3	100.9	100.5
Cations calculated on the basis of 4 oxygens					
Fe	0.21	0.24	0.21	0.20	0.21
Mn	0.00	0.00	0.00	0.00	0.00
Ni	0.01	0.01	0.01	0.01	0.01
Mg	1.78	1.75	1.78	1.79	1.78
Fo	89	88	89	90	89

5.3. Origin of the plagioclase megacrysts

As pointed by Laughlin et al. (1974), two possibilities exist for the origin of the plagioclase megacrysts: (1) the megacrysts are accidental xenocrysts and there is no relation between these megacrysts and host basalt; and (2) the megacrysts are cognate phenocrysts, having crystallized under particular pressure and temperature conditions as the basalts rose to the surface.

If the plagioclase megacrysts were accidental xenocrysts, they would have fragmented or irregular edges, whereas these plagioclases are euhedral with sharp margins and they are not corroded. In addition they would have had to have been derived from some source such as anorthosite or pegmatites, whereas there is no exposure of these rocks in this area. The closest source possibly to provide sodic plagioclase is the Precambrian granite gneiss cropping out in a few kilometers to the south and southeast (Fig. 1). The lavas most likely passed through these gneisses, but the $^{87}Sr/^{86}Sr$ ratio of the plagioclase megacrysts, which is 0.704596 (Table 4), is too low for a Precambrian rock. Alternatively the feldspar crystals might be completely re-equilibrated with the strontium in the basaltic melt (Laughlin et al., 1974), but the high strontium content of the plagioclase megacrysts (2800 ppm) and relatively low strontium content in the basalt (570–778 ppm) are inconstant

Table 6b
Compositions of Cr-diopside clinopyroxene in pyroxenites.

Lithotype	Pyroxenite				
Sample	NXP 9	NXP 1-2	NXP 11-1	Na (CPX)	Nb (CPX)
No.	4	4	4	4	4
SiO_2	53.8	53.8	53.0	53.2	53.1
TiO_2	0.1	0.1	0.2	0.2	0.1
Al_2O_3	1.9	2.6	1.7	2.1	1.3
Cr_2O_3	1.0	0.5	0.2	0.8	0.6
FeO	3.0	4.2	4.7	2.9	3.3
MnO	0.1	0.2	0.1	0.1	0.2
MgO	17.2	16.6	17.1	16.8	17.3
CaO	22.5	22.2	22.6	22.0	22.3
Na_2O	0.5	0.6	0.3	0.7	0.3
Total	100.2	100.5	100.0	98.8	98.4
Cations calculated on the basis of 6 oxygens					
Si	1.95	1.95	1.96	1.96	1.96
Al	0.08	0.11	0.07	0.09	0.06
Ti	0.00	0.00	0.01	0.00	0.00
Cr	0.03	0.01	0.01	0.02	0.02
Fe	0.09	0.13	0.14	0.09	0.10
Mn	0.00	0.01	0.01	0.00	0.00
Mg	0.93	0.90	0.92	0.92	0.95
Ca	0.88	0.86	0.88	0.87	0.88
Na	0.04	0.04	0.02	0.05	0.02
En	49	47	48	49	49
Wo	46	46	45	46	46
Fs	5	7	7	5	5
Mg#	92	89	88	92	92

Table 6a
Compositions of Cr-diopside clinopyroxene in lherzolite.

Lithotype	Lherzolite				
Sample	NXP 3-3	NXP 10	NXP 11-2	NXP 5	NXP 1
No.	3	3	3	3	4
SiO_2	52.3	51.8	51.8	50.8	50.8
TiO_2	0.3	0.5	0.6	0.5	0.7
Al_2O_3	5.3	7.1	6.7	6.8	7.2
Cr_2O_3	1.0	0.9	0.7	0.7	0.4
FeO	2.5	2.8	2.8	2.9	2.7
MnO	0.1	0.1	0.1	0.1	0.1
MgO	16.0	15.1	15.7	15.5	15.4
CaO	20.7	18.9	20.5	19.9	20.3
Na_2O	1.4	2.1	1.6	1.8	1.8
Total	99.6	99.3	100.6	99.0	99.2
Cations calculated on the basis of 6 oxygens					
Si	1.89	1.86	1.86	1.85	1.84
Al	0.22	0.31	0.28	0.29	0.31
Ti	0.01	0.01	0.02	0.01	0.02
Cr	0.03	0.03	0.02	0.02	0.01
Fe	0.07	0.06	0.09	0.09	0.09
Mn	0.00	0.00	0.00	0.00	0.00
Mg	0.86	0.82	0.84	0.84	0.82
Ca	0.80	0.74	0.79	0.77	0.79
Na	0.10	0.15	0.11	0.12	0.13
En	50	50	49	50	49
Wo	46	45	46	45	46
Fs	4	5	5	5	5
Mg#	93	92	92	92	93

Table 7a
Compositions of orthopyroxene in lherzolites.

Lithotype	Lherzolite				
Sample	NXP 10	NXP 11-2	NXP 5	NXP 1	NXP 3-3
No.	3	3	4	3	3
SiO_2	54.1	55.8	54.5	55.8	55.0
Al_2O_3	4.6	4.4	4.8	3.9	3.6
Cr_2O_3	0.4	0.3	0.3	0.3	0.4
FeO	6.3	6.4	6.6	6.8	5.8
MnO	0.1	0.1	0.1	0.2	0.1
MgO	32.6	33.3	33.0	32.6	33.6
CaO	0.8	0.8	0.8	0.8	0.7
Na_2O	0.2	0.1	0.1	0.1	0.1
Total	99.1	101.2	100.4	100.4	99.6
Cations calculated on the basis of 6 oxygens					
Si	1.88	1.90	1.87	1.92	1.90
Al	0.19	0.18	0.20	0.16	0.15
Cr	0.01	0.01	0.01	0.01	0.01
Fe	0.18	0.18	0.19	0.20	0.17
Mn	0.00	0.00	0.00	0.00	0.00
Mg	1.69	1.69	1.70	1.68	1.74
Ca	0.03	0.03	0.03	0.03	0.03
Na	0.01	0.01	0.01	0.01	0.01
En	89	89	88	88	90
Wo	2	1	2	2	1
Fs	9	10	10	10	9
Mg#	92	92	91	91	92

Table 7b
Compositions of orthopyroxene in pyroxenites.

Lithotype	Pyroxenite		
Sample	NXP 9	NXP 1-2	NXP 11-1
No.	4	4	4
SiO_2	56.5	56.1	56.3
Al_2O_3	1.5	2.1	1.4
Cr_2O_3	0.5	0.2	0.1
FeO	7.4	9.6	10.5
MnO	0.2	0.2	0.3
MgO	33.4	31.5	31.3
CaO	0.7	0.8	0.8
Total	100.2	100.4	100.8
Cations calculated on the basis of 6 oxygens			
Si	1.96	1.95	1.98
Al	0.06	0.09	0.10
Cr	0.02	0.01	0.00
Fe	0.21	0.29	0.30
Mn	0.01	0.01	0.00
Mg	1.73	1.65	1.63
Ca	0.03	0.02	0.00
En	88	84	83
Wo	1	1	2
Fs	11	14	15
Mg#	90	87	86

with this process. Plagioclase of lower crustal xenoliths varies from An_{44-51} (Table 11) whereas the megacrysts are more sodic, between An_{26-32} (Fig. 4), indicating that the megacrysts were not formed from these xenoliths.

Thus we conclude that the plagioclase megacrysts have a cognate origin with the host basalt. Wright (1968) reported large crystals of oligoclase and andesine in alkaline basalts from Nigeria which are distinctly more sodic than plagioclase microlites in the rock. Aoki (1970) also reported sodic plagioclase megacrysts in Japanese alkaline basalts. The compositional range of plagioclase in host rock varies from An_{28-59} (Table 1) whereas this range for megacrysts is more sodic between An_{26-32} (Fig. 4). It seems therefore that there were two different conditions for the generation of feldspar phenocrysts and megacrysts in the basaltic host rock. Based on the numerous experimental studies by Cohen et al. (1967), Green and Ringwood (1967) and a comprehensive study of megacrysts in alkaline lavas by Binns et al. (1970) there is a tendency of plagioclase to become more sodic at high pressures. Aoki (1970) also concluded that the sodic plagioclase megacrysts in Japanese alkali basalts result from high-pressure crystallization at depths of 30–60 km.

Melt partition coefficients for trace elements provide a useful tool to examine equilibrium condition between plagioclase megacrysts and an alkaline basalt host rock. The partition coefficients (kD) between basalt (liquid phase) and plagioclase (crystal phase) based on the trace elements analysis of our samples are compared with the partitioning of trace elements between crystal and melt based on experimental and natural data in Table 12. The general pattern of

Table 8
Trace element composition (in ppm) for clinopyroxene from pyroxenite Nb (CPX).

Nb (CPX)									
Ni	201	Sr	62	Y	3.8	Nd	1.69	Zr/Nb	3.15
Cr	3979	Nb	2.4	Hf	1.1	Sm	0.60	La/Nb	0.21
V	151	Ta	2.7	Tb	0.1	Eu	0.21	Y/Nb	1.59
Rb	2.5	Zr	7.4	La	0.57	Tb	0.10	$(La/Yb)_N$	3.65
Ba	0.7	Ti	1344	Ce	1.84	Yb	0.28	Mg#	92

Table 9
Composition of amphibole in peridotite xenolith NXP 4.

NXP-4					
SiO_2	41.9	42.6	*Number of cations on basis of 23 oxygens*		
TiO_2	3.9	3.4	Si	6.07	6.16
Al_2O_3	14.6	14.4	Ti	0.42	0.4
FeO	4.6	4.4	Al	2.49	2.44
MnO	0.1	0.1	Fe	0.56	0.53
MgO	16.5	16.8	Mg	3.57	3.63
CaO	10.9	10.8	Mn	0.01	0.01
Na_2O	3.4	3.3	Ca	1.68	1.68
K_2O	1.4	1.4	Na	0.94	0.92
Cl	0.0	0.0	K	0.26	0.26
F	3.2	3.2	Cl	0.01	0.01
Total	100.4	100.4	F	1.47	1.47

distribution of selected elements versus plagioclase and basalt partition coefficient is relatively higher but similar to those from published references (Fig. 12). The composition of plagioclase in the references data might be a little different from the samples of this study, accounting for at least part of this variation. Thus, we concluded that the Iranian plagioclase megacrysts could be crystallized from the host rock alkali basalt.

Aigner-Torres et al. (2007) used laser ablation ICP-MS to study plagioclase-melt partition coefficient at three temperatures (1220, 1200, and 1180 °C) and at different oxygen fugacities. It seems that the plagioclase-melt partition coefficients at 1180 °C and log $fO = -12.19$ are the best match with the composition of plagioclase megacryst and alkaline basaltic host rock in northeastern Iran (Fig. 12).

The measured $^{87}Sr/^{86}Sr$ ratio of the plagioclase megacrysts is 0.704596 which is lower than the alkali basalt host rock (Table 4), consistent with differences among megacrysts and host basalts

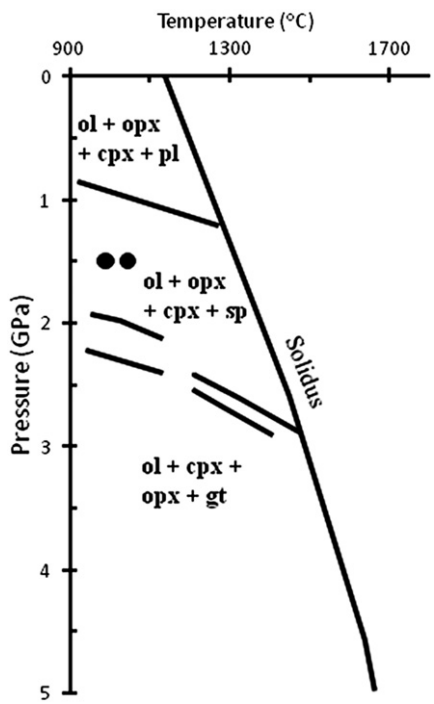

Fig. 9. Pressure–temperature diagram illustrating the temperature conditions of equilibration at 15 kbars of a mantle lherzolite and a pyroxenite xenolith within the northeastern Iran basalts. Peridotite solidus and phase boundaries after Pearson et al. (2003) and references therein.

Table 10
Equilibrium temperature estimates of selected peridotite xenoliths, using the Brey and Kohler (1990) formulation for the two-pyroxene geothermometer at 15 kbars.

Lithotype	Pyroxenite								Lherzolith					
Sample	NXP 9				NXP 11-1				NXP 11-2			NXP 10		
	Core	Rim	Core	Rim	Core	Rim	Core	Rim	Core	Rim	Core	Core	Rim	Core
10 kbar	966	972	973	967	994	973	971	965	980	982	1005	1004	1002	1009
15 kbar	990	997	998	992	990	997	996	990	1004	1006	1030	1029	1027	1034
20 kbar	1015	1021	1022	1016	1015	1022	1020	1014	1029	1031	1055	1054	1053	1059
Lithotype	Lherzolith													
Sample	NXP 1-2				NXP 5				NXP 3-3			NXP 1		
	Core	Rim	Core	Rim	Core	Rim	Core	Rim	Core	Rim	Core	Core	Rim	Core
10 kbar	987	997	980	995	1008	1005	1018	1015	982	985	979	980	999	982
15 kbar	1012	1022	1005	1020	1034	1031	1044	1040	1006	1010	1004	1004	1024	1007
20 kbar	1037	1047	1030	1045	1059	1056	1069	1065	1031	1035	1029	1029	1049	1031

reported elsewhere in the literature. For example, Aspen et al. (1990) reported $^{87}Sr/^{86}Sr$ values of alkali feldspar megacrysts and alkali basalts from Scotland which indicate that the megacrysts also had the lower value, and according to Dasch (1969), this ratio for anorthoclase crystals (0.7024) taken from a basalt in Texas is lower than their basaltic matrix (0.70410). Two of the Bandera anorthoclases (New Mexico), occurring within a basaltic host with mean $^{87}Sr/^{86}Sr$ ratio of 0.7031, also had lower values of 0.7027 and 0.7029 (Laughlin et al., 1974). Irving and Frey (1984) pointed out that in most, but not all cases the megacrysts in a basaltic host have lower $^{87}Sr/^{86}Sr$ ratio than the basalt, and suggested that the possibility of crustal contamination or secondary alteration of the basalt after crystallization of the megacrysts must be considered as an explanation for this.

5.4. Source of mantle xenoliths

The spinel lherzolite and pyroxenite mantle xenoliths within the basalts indicate a range of temperature between 966 and 1069 °C using the two pyroxene geothermometer (Brey and Kohler, 1990) and assuming an equilibrium pressure of 15 kbar (Table 10; Fig. 9). A maximum pressure estimate of the studied xenolith samples, based on the mineral assemblage and particularly absence of garnet, would be about 19 kbar (e.g., Miller, 1982). An approximate minimum pressure, based on the thickness of crust in this area (~42 km, Mokhtari et al., 2004) is only around 13 kbar. The temperature determined is lower than the temperatures (~1300 °C) expected for the convecting asthenospheric mantle. This, as well as their granular textures, indicates that the mantle xenoliths from northeastern Iran are derived from the

Table 11
Compositions of pyroxenes, plagioclase and olivine in crustal gabbroic xenoliths and plagioclase megacrysts.

Crustal xenoliths									Megacryst		
Sample	NXG 1			NXG 1	NXG 2	NXG 3	NXG 3			NXM 1	NXM 2	NXM 3
Mineral	OPX	CPX	Plag.				Olivine		Plag.			
No.	3	4		1	1	1		3		1	1	4
SiO_2	50.5	50.4	SiO_2	56.4	57.1	57.3	SiO_2	36.2	SiO_2	61.9	61.0	60.8
TiO_2	0.2	0.5	Al_2O_3	26.9	27	27	FeO	31.0	Al_2O_3	24.8	24.4	24.1
Al_2O_3	3.1	3.5	FeO	0.3	0.4	0.3	MnO	0.8	FeO	0.2	0.2	0.2
FeO	21.6	10.9	CaO	8.7	8.6	8.7	MgO	30.2	CaO	5.7	5.5	5.4
MnO	0.6	0.3	Na_2O	5.5	5.7	5.6	Total	98.4	Na_2O	5.8	7.3	7.2
MgO	20.8	13.0	K_2O	1.2	1	1.2			K_2O	1.4	1.7	1.5
CaO	1.1	18.7	Total	98.9	99.7	100.1	*Cations calculated on the basis of 4 oxygens*		Total	99.8	100.2	99.3
Na_2O	0.0	0.6					Fe	0.96				
Total	98.0	97.9	*Cations calculated on basis of 32 oxygens*				Mn	0.03	*Cations calculated on basis of 32 oxygens*			
			Si	10.27	10.3	10.31	Mg	1.67	Si	11.2	10.87	10.96
Cations calculated on the basis of 6 oxygens			Al	5.77	5.75	5.72			Al	5.29	5.13	5.12
Si	1.92	1.92	Fe	0.05	0.05	0.04	Fo	63	Fe	0.03	0.03	0.03
Al	0.14	0.16	Ca	1.7	1.67	1.68			Ca	1.1	1.05	1.04
Ti	0.00	0.02	Na	1.94	2	1.96			Na	2.05	2.53	2.50
Fe	0.69	0.35	K	0.28	0.23	0.28			K	0.33	0.38	0.35
Mn	0.02	0.01										
Mg	1.18	0.74	Or	7	7	8			Or	9	10	9
Ca	0.04	0.76	Ab	50	60	59			Ab	59	64	64
Na	0.00	0.05	An	44	50	51			An	32	26	27
En	62	40										
Wo	2	41										
Fs	36	19										
Mg#	67	71										

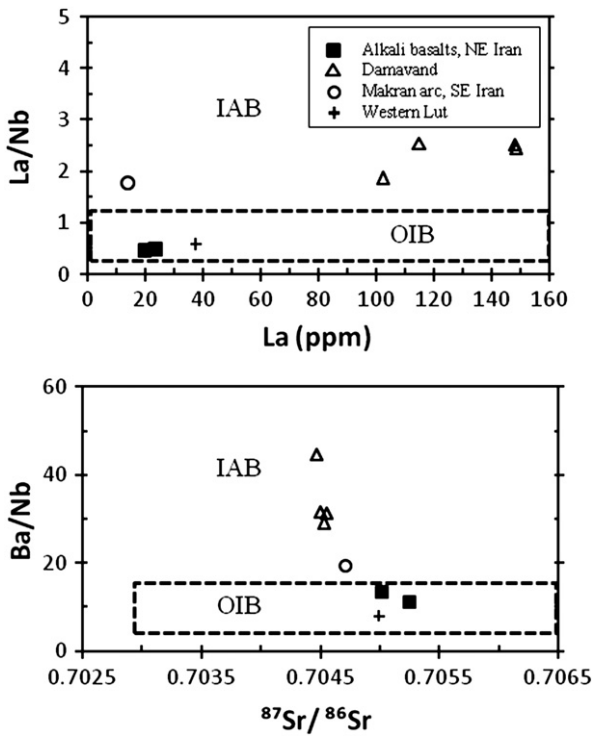

Fig. 10. La/Nb versus La concentration and Ba/Nb versus $^{87}Sr/^{86}Sr$ for samples of alkali basalts from northeastern Iran, Makran arc and Damavand volcano basalts. The limits of the field of oceanic island basalt (OIB) and MORB from Hickey-Vargas et al. (1986), and the other data from the references mentioned above.

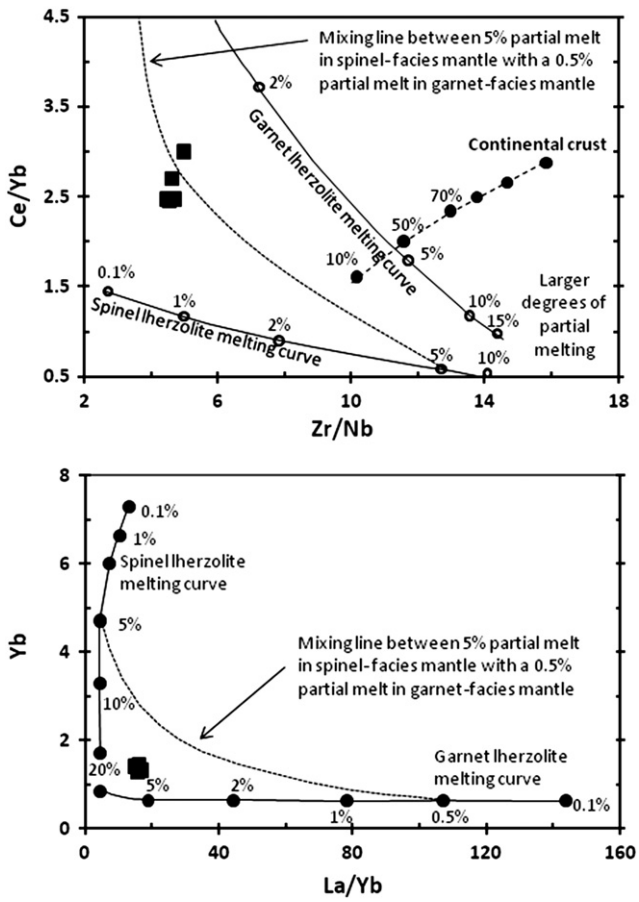

Fig. 11. Variation of Zr/Nb vs Ce/Y and Yb versus La/Yb for the northeastern Iran samples compared to non-modal, fractional melting curves for spinel (0·578 Ol, 0·270 Opx, 0·119 Cpx, 0·033 Sp that melts in the proportions 0·10 Ol, 0·27 Opx, 0·50 Cpx, 0·13 Sp) and garnet lherzolite (0·598 Ol, 0·211 Opx; 0·076 Cpx, 0·115 Gt that melts in the proportions 0·05 Ol, 0·20 Opx, 0·30 Cpx, 0·45 Gt), and for an upper-crustal estimate taken from Baker et al. (1997).

lithospheric mantle and undoubtedly the depth of formation of the host magma must exceed the source of the maximum pressure of xenoliths.

Pyroxenite xenoliths may have crystallized from mafic basaltic magma at high pressure (Wilshire and Shervais, 1975; Frey and Prinz, 1978; Pearson et al., 2003). We have calculated the trace-element composition of the hypothetical melts from which they have crystallized using cpx/melt partition coefficients and the composition of a clinopyroxene separated from a pyroxenite sample. Partition coefficients depend on several parameters like temperature (T), pressure (P), composition (X), and oxygen fugacity (fO_2). We used partition coefficient reported by Hart and Dunn (1993) since their cpx/melt partitioning data is about in the middle of the published range (Frey et al., 1978; Irving, 1978; Hart and Dunn, 1993). Chondrite-normalized diagram for rare-earth elements (REE) of a clinopyroxene separated from a pyroxenite xenolith and the calculated parental melts are shown in Fig. 13. The chondrite-normalized pattern for REE of the calculated parental melts follows the same trend of the patterns of the host basalt, but the concentrations are much lower suggesting that they crystallized from a less alkaline melt. Also, they also have higher Nd and lower Sr isotope ratios than host alkaline basalts (Fig. 8, Table 4). Consequently the xenoliths probably crystallized from older basaltic magmas, possibly during the more voluminous episode of magmatism than occurred in this region during the early to mid-Tertiary.

According to Liotard et al. (2008) the Damavand volcano, located in northern Iran around 1000 km to the west, is characterized by low degree of partial melting (~5%) of a garnet and phlogopite-rich lherzolite highly-metasomatized mantle source. In contrast, the mantle xenolith samples of northeastern Iran do not show any unusual mineralogy or textures, other than the presence of pyroxenites and the fact that one sample contains amphibole (Table 9). We conclude that the mantle below northeastern Iran has not been metasomatized by highly alkaline fluids, although the presence of pyroxenites suggests the previous through-passage of basaltic magmas in this region.

5.5. Conclusions

The presence of the Neogene alkali basalt cone at the intersection of the E–W and N–S faults that bound the Lut block, as well as along these faults to the south and west (Saadat et al., 2010) is consistent with the continued persistence of hot mantle below this area of eastern Iran, although the volume of Neogene volcanic rocks is much smaller than in the Eocene and Oligocene, and volcanism is now restricted to only along these deep structures. These alkali basalts are all similar to oceanic island basalts (OIB) and their genesis does not require extensive metasomatism of the underlying continental mantle lithosphere as has been invoked for the genesis of the magmas erupted from Damavand volcano further to the west in Iran (Liotard et al., 2008). Mantle xenoliths within these alkali basalts also do not show signs of extensive metasomatism, implying significant regional difference in the chemical evolution of the Iranian subcontinental lithospheric mantle.

Acknowledgment

This study is part of the first author's Ph.D. dissertation at University of Colorado, Boulder, USA. Financial support was provided by the

Table 12
Partition coefficients for a plagioclase megacryst and basalt (Table 3) compared with published plagioclase/melt partition coefficients (kD).

	Bulk rock (ppm)	Plag. (ppm)	Cp/Cb (kD)	Reference (kD)		Bulk rock (ppm)	Plag. (ppm)	Cp/Cb (kD)	Reference (kD)
Ti	10,847	582	0.054	0.038	Ba	512	463.00	0.903	0.30
V	156	88	0.567	0.10	Y	14	0.83	0.059	–
Cr	66	5	0.084	–	Zr	217	1.41	0.006	–
Mn	1096	18	0.016	0.053	La	17	5.09	0.287	0.135
Co	34	2	0.060	–	Ce	37	6.55	0.179	0.09
Ni	77	23	0.302	–	Pr	4	0.53	0.126	0.17
Cu	22	3	0.119	–	Nd	18	1.79	0.098	0.04
Zn	126	30	0.237	–	Sm	4	0.52	0.127	0.036
Rb	25	14	0.565	0.016	Eu	1.5	2.29	1.510	0.32
Sr	546	2801	5.127	2.94	Gd	4	0.24	0.055	0.04

kD reference data for Sr, La, Mn, Rb, Ba, Ce, Nd, Sm, Eu and Gd from Matsui et al. (1977); Ca from Higuchi and Nagasawa (1969); Ti and V from Bougault and Hekinian (1974); Cs from Villemant et al. (1981); Nb and Pr from McKenzie and O'Nions (1991).

Society of Economic Geology (SEG) and the Department of Geological Sciences at CU. Thanks to Lang Farmer and Emily Verplanck for access to TIMS lab and their help in obtaining the isotopic data for this study, John Drexler for assistance with the electron microprobe, and to Karl Mueller for preparing the satellite image. We are grateful to Abbasnia, Saadati, Ghoorchi, Soroush and Fatemeh for their field assistance.

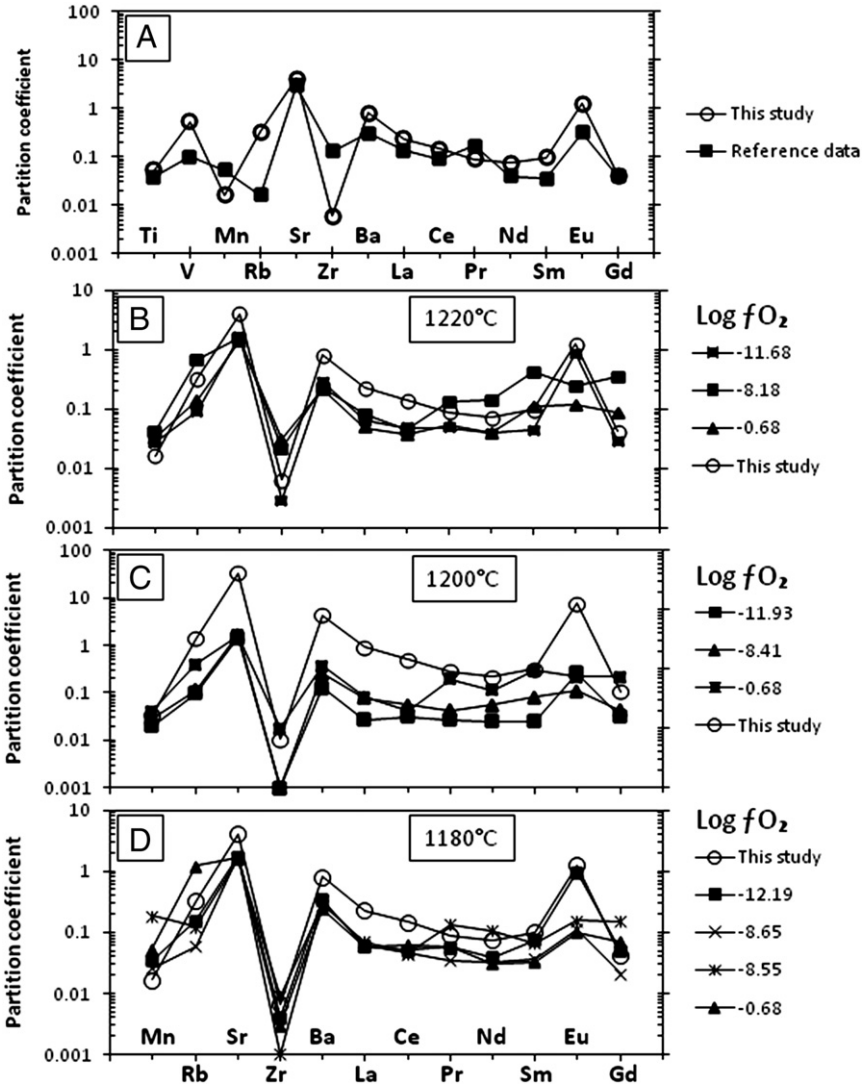

Fig. 12. (A) Plot of partition coefficient for selected elements for the basaltic (liquid phase) host and the plagioclase (crystal phase) megacrysts from northeast Iran, compared to mineral–melt partitioning coefficients from the Geochemical Earth Reference Model (GERM) website (http://earthref.org/GERM/). (B, C and D) Partition coefficient at several temperatures and oxygen fugacities from Aigner-Torres et al. (2007) compared with samples from this study.

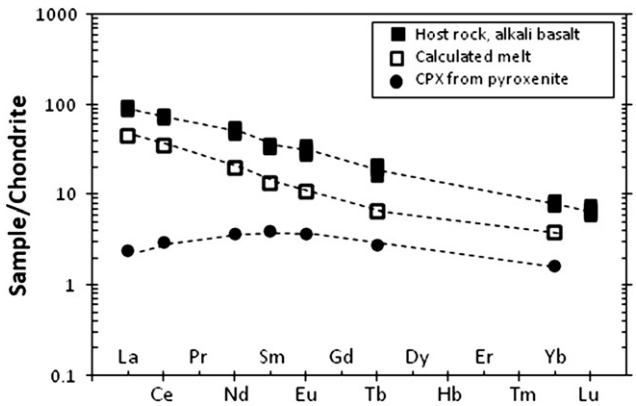

Fig. 13. Comparison of calculated parental melt trace element contents (empty square) coexisting with clinopyroxenes in pyroxenite xenoliths (solid circle) found in the alkali basalts (solid square) from northeastern Iran. Melt compositions were calculated using the partition coefficients La = 0.0536; Ce = 0.0858; Nd = 0.1873; Sm = 0.291; Eu = 0.338; Tb = 0.429; Yb = 0.430; Lu = 0.435 from Hart and Dunn (1993). Chondrite values are from Sun and McDonough (1989).

References

Aigner-Torres, M., Blundy, J., Ulmer, P., 2007. Laser Ablation ICPMS study of trace element partitioning between plagioclase and basaltic melts: an experimental approach. Contributions to Mineralogy and Petrology 153, 647–667.

Alavi, M., 1979. The Virani ophiolite complex and surrounding rocks. Geologische Rundschau 68 (1), 334–341.

Alicic, P., Temel, A., Gourgaud, A., 2002. Pb–Nd–Sr isotope and trace element geochemistry of Quaternary extension-related alkaline volcanism: a case study of Kula region (western Anatolia, Turkey). Journal of Volcanology and Geothermal Research 115, 487–510.

Al-Lazki, A.I., Sandvol, E., Seber, D., Barazangi, M., Turkelli, N., Mohamad, R., 2004. Pn tomographic imaging of mantle lid velocity and anisotropy at the junction of the Arabian, Eurasian, and African plates. Geophysical Journal International 158 (3), 1024–1040.

Ambraseys, N., Bilham, R., 2003. Earthquakes in Afghanistan. Seismological Research Letters 74 (2), 107–123.

Aoki, K., 1970. Andesine megacrysts in alkali basalts from Japan. Contributions to Mineralogy and Petrology 25, 284–288.

Aspen, P., Upton, B.G.J., Dickin, A.P., 1990. Anorthoclase, sanidine and associated megacrysts in Scottish alkali basalts: high-pressure syenitic debris from upper mantle sources. European Journal of Mineralogy 2, 503–517.

Baker, J.A., Menzies, M.A., Thirlwall, M.F., MacPherson, C.G., 1997. Petrogenesis of Quaternary intraplate volcanism, Sana'a, Yemen: implications for plume–lithosphere interaction and polybaric melt hybridization. Journal of Petrology 38 (10), 1359–1390.

Beard, B.L., Johnson, C.M., 1997. Hafnium isotope evidence for the origin of Cenozoic basaltic lavas from the southwestern United States. Journal of Geophysical Research 102, 20149–20178.

Binns, R.A., Duggan, M.D., Wilkinson, J.G.F., 1970. High pressure megacrysts in alkaline lavas from northeastern New South Wales. American Journal of Science 269, 132–168.

Bougault, H., Hekinian, R., 1974. Rift valley in the Atlantic Ocean near 36 degrees 50′N; petrology and geochemistry of basalt rocks. Earth and Planetary Science Letters 24 (2), 249–261.

Brey, G.P., Kohler, T., 1990. Geothermobarometry in four-phase lherzolites II. New thermobarometers, and practical assessment of existing thermobarometers. Journal of Petrology 31 (6), 1353–1378.

Brunet, M.F., Korotaev, M.V., Ershov, A.V., Nikishin, A.M., 2003. The South Caspian Basin: a review of its evolution from subsidence modelling. Sedimentary Geology 156, 119–148.

Cohen, L.H., Ito, K., Kennedy, G.C., 1967. Melting and phase relations in anhydrous basalts to 40 kilobars. American Journal of Science 265, 475–518.

Dasch, E.J., 1969. Strontium isotope disequilibrium in a porphyritic alkali basalt and its bearing on magmatic processes. Journal of Geophysical Research 74 (2), 560–565.

Dobosi, G., Jenner, G.A., Embey-Isztin, A., Downes, H., 2010. Cryptic metasomatism in clino- and orthopyroxene in the upper mantle beneath the Pannonian region. Petrological Evolution of the European Lithospheric Mantle: Special Publication, 337. The Geological Society of London, pp. 177–194.

Fakhari, M.D., Axen, G.J., Horton, B.K., Hassanzadeh, J., Amini, A., 2008. Revised age of proximal deposits in the Zagros foreland basin and implications for Cenozoic evolution of the High Zagros. Tectonophysics 451 (1–4), 170–185.

Farmer, G.L., 2003. Continental basaltic rocks. Treatise on Geochemistry 3, 1–39.

Farmer, G.L., Broxton, E.D., Warren, G.R., Pickthon, W., 1991. Nd, Sr, and O isotopic variations in metaluminous ash-flow tuffs and related volcanic rocks at Timber Mountain/Oasis Valley Caldera, Complex, Sw Nevada: implication for the origin and evolution of large-volume silicic magma bodies. Contributions to Mineralogy and Petrology 109, 53–68.

Farmer, G.L., Glazner, A.F., Manley, C.R., 2002. Did lithospheric delamination trigger late Cenozoic potassic volcanism in the southern Sierra Nevada, California. GSA Bulletin 114 (6), 754–768.

Frey, F.A., Prinz, M., 1978. Ultramafic inclusions from San Carlos, Arizona: petrologic and geochemical data bearing on their petrogenesis. Earth and Planetary Science Letters 38, 129–176.

Frey, F.A., Green, D.H., Roy, S.D., 1978. Integrated models of basalt petrogenesis: a study of quartz tholeiites to olivine melilitites from southeastern Australia utilizing geochemical and experimental petrologic data. Journal of Petrology 19, 463–513.

Gast, P.W., 1968. Trace element fractionation and the origin of tholeiitic and alkaline magma types. Geochemica Cosmochimica Acta 32, 1057–1086.

Gautheron, C., Moreira, M., Allègre, C., 2005. He, Ne and Ar composition of the European lithospheric mantle. Chemical Geology 217, 97–112.

Geochemical Earth Reference Model (GERM), website: http://earthref.org/GERM/.

Geologic Survey of Iran, 1984. Kariz-Now, Geological Map, 1:100000. Geological Survey of Iran, Tehran.

Golonka, J., 2000. Geodynamic evolution of the south Caspian Basin. AAPG's Inaugural Regional International Conference, Istanbul, Turkey, pp. 40–45.

Golonka, J., 2004. Plate tectonic evolution of the southern margin of Eurasia in the Mesozoic and Cenozoic. Tectonophysics 381, 235–273.

Green, D.H., Ringwood, A.E., 1967. The genesis of basaltic magmas. Contributions to Mineralogy and Petrology 15, 103–190.

Haase, K.M., 1996. The relationship between the age of the lithosphere and the composition of oceanic magmas: constraints on partial melting, mantle sources and the thermal structure of the plates. Earth and Planetary Science Letters 144, 75–92.

Hart, S.R., 1984. A large-scale isotope anomaly in the Southern Hemisphere mantle. Nature 309, 753–757.

Hart, S.R., Dunn, T., 1993. Experimental cpx/melt partitioning of 24 trace elements. Contributions to Mineralogy and Petrology 113, 1–8.

Hart, S.R., Gunn, B.M., Watkins, N.D., 1971. Interlava variation of alkali elements in Icelandic basalt. American Journal of Science 270, 315–318.

Hassanzadeh, J., Axen, G., Guest, B., Stockli, D.F., Ghazi, A.M., 2004. The Alborz and NW Urumieh–Dokhtar magmatic belts, Iran: rifted parts of a single ancestral arc. Geological Society of America National Meeting. Geological Society of America, Denver, Colorado, p. 434.

Hassanzadeh, J., Stockli, D.F., Horton, K.B., Axen, J.G., Stockli, D.L., Grove, M., Schmitt, K.A., Walker, J.D., 2008. U–Pb zircon geochronology of late Neoproterozoic–Early Cambrian granitoids in Iran: implications for paleogeography, magmatism, and exhumation history of Iranian basement. Tectonophysics 451, 71–96.

Hibbard, M.J., 1995. Petrography to Petrogenesis. Prentice-Hall, Inc.. 587 pp.

Hickey-Vargas, R.L., Frey, F.A., Gerlach, D.C., López-Escobar, L., 1986. Multiple sources for basaltic arc rocks from the Southern Volcanic Zone of the Andes (34°–41°S): trace element and isotopic evidence for contributions from subducted oceanic crust, mantle and continental crust. Journal of Geophysical Research 91 (6), 5963–5983.

Higuchi, H., Nagasawa, H., 1969. Partition of trace elements between rock-forming minerals and the host volcanic rocks. Earth and Planetary Science Letters 7, 281–287.

Hirose, K., Kushiro, I., 1993. Partial melting of dry peridotites at high pressures: determination of compositions of melts segregated from peridotite using aggregates of diamond. Earth and Planetary Science Letters 114, 477–489.

Hofmann, A.W., 1997. Mantle geochemistry: the message from oceanic magmatism. Nature 385, 219–229.

Horton, B.K., Hassanzadeh, J., Stockli, D.F., Axen, G.J., Gillis, R.J., Guest, B., Amini, A.H., Fakhari, M., Zamanzadeh, S.M., Grove, M., 2008. Detrital zircon provenance of Neoproterozoic to Cenozoic deposits in Iran: implications for chronostratigraphy and collisional tectonics. Tectonophysics 451, 97–122.

Irving, A.J., 1978. A review of experimental studies of crystal/liquid trace element partitioning. Geochemica Cosmochimica Acta 42, 743–770.

Irving, A.J., Frey, F.A., 1984. Trace clement abundances in megacrysts and their host basalts: constraints on partition coefficients and megacryst genesis. Geochimica et Cosmochimica Acta 48, 1201–1221.

Jackson, J., 1992. Partitioning of strike-slip an convergent motion between Eurasia and Arabia in eastern Turkey and Arabia. Journal of Geophysical Research 97, 12479–12741.

Jackson, J., McKenzie, D., 1984. Active tectonics of the Alpine–Himalayan belt between western Turkey and Pakistan. Geophysics Journal of the Royal Astronomical Society 77, 185–264.

Kargaran, F., Neubauer, F., Genser, J., Houshmandzadeh, A., 2006. The Eocene Chapedony metamorphic core complex in central Iran: preliminary structural results. European Geosciences Union Geophysical Research Abstracts 8.

Kesson, S.E., 1973. The primary geochemistry of the Monaro Alkaline Volcanics, southeastern Australia, evidence for upper mantle heterogeneity. Contributions to Mineralogy and Petrology 42, 93–108.

Kheirkhah, M., Allen, M.B., Emami, M., 2009. Quaternary syn-collision magmatism from the Iran/Turkey borderlands. Journal of Volcanology and Geothermal Research 182, 1–12.

Kopp, M.L., 1997. Lateral escape structures in the Alpine–Himalayan collision belt (in Russian). Russian Academy of Sciences Transactions 506, 1–314.

Langmuir, C.H., Klein, E.M., Plank, T., 1992. Petrological systematics of mid-ocean ridge basalts: constraints on melt generation beneath ocean ridges. Geophysical Monograph, 71. American Geophysical Union, Washington DC, pp. 183–280.

Laughlin, A.W., Manzer, G.K., Carden, L.R., 1974. Feldspar megacrysts in alkali basalts. Geological Society of America Bulletin 85, 413–416.

Le Maitre, R.W. (editor), Streckeisen, A., Zanettin, B., Le Bas, M.J., Bonin, B., Bateman, P., Bellieni, G., Dudek, A., Efremova, S., Keller, J., Lameyre, J., Sabine, P.A., Schmid, R., Sorensen, H., Woolley, A.R., 2002. Igneous Rocks: A Classification and Glossary of Terms, Recommendations of the International Union of Geological Sciences, Subcommission of the Systematics of Igneous Rocks. Cambridge University Press, 236 pp.

Liotard, J.M., Dautria, J.M., Bosch, D., Condomines, M., Mehdizadeh, H., Ritz, J.F., 2008. Origin of the absarokite–banakite association of the Damavand volcano (Iran): trace elements and Sr, Nd, Pb isotope constraints. International Journal of Earth Sciences (Geologische Rundschau) 97, 89–102.

Lloyd, F.E., 1987. Characterization of mantle metasomatic fluids in spinel lherzolites and alkali clinopyroxenites from the West Eifel and Southwest Uganda. In: Menzies, M.A., Hawkesworth, C.J. (Eds.), Mantle metasomatism: Geology Series. Academic Press, London, pp. 91–121.

Lloyd, F.E., Bailey, D.K., 1975. Light element metasomatism of the continental mantle: the evidence and consequences. Physical Chemistry of the Earth 9, 389–416.

Matsui, Y., Onuma, N., Nagasawa, H., Higuchi, H., Banno, S., 1977. Crystal structure control in trace element partition between crystal and magma. Tectonics 100, 315–324.

McKenzie, D., O'Nions, R.K., 1991. Partial melt distributions from inversion of rare earth element concentrations. Journal of Petrology 32, 1021–1091.

Middlemost, E.A.K., 1975. The basalt clan. Earthscience Reviews 11, 337–364.

Miller, C., 1982. Geochemical constrains on the origin of xenolith-bearing alkali basaltic rocks and megacryst from the Hoggar, central Sahara. Geochemical Journal 16, 225–236.

Mokhtari, M., Farahbod, A.M., Lindholm, C., Alahyarkhani, M., Bungum, H., 2004. An approach to a comprehensive Moho depth map and crust and upper mantle velocity model for Iran. Iranian International Journal of Science 5 (2), 223–244.

Moritz, R., Ghazban, F., Singer, B.S., 2006. Eocene Gold Ore Formation at Muteh, Sanandaj–Sirjan Tectonic Zone, Western Iran: a result of late-stage extension and exhumation of metamorphic basement rocks within the Zagros orogen. Economic Geology 101 (8), 1497–1524.

Nasir, S., Al-Sayigh, A., Alharthy, A., Al-Lazki, A., 2006. Geochemistry and petrology of Tertiary volcanic rocks and related ultramafic xenoliths from the central and eastern Oman Mountains. Lithos 90, 249–270.

Pearce, J.A., 1996. Sources and settings of granitic rocks. Episodes 19 (4), 120–125.

Pearce, J.A., Bender, J.F., De Long, S.E., Kidd, W.S.F., Low, P.J., Gijner, Y., Saroglu, F., Yilmaz, Y., Moorbathg, S., Mitchell, J.G., 1990. Genesis of collision volcanism in Eastern Anatolia, Turkey. Journal of Volcanology and Geothermal Research 44, 189–229.

Pearson, D.G., Canil, D., Shirey, S.B., 2003. Mantle samples included in volcanic rocks: xenoliths and diamonds. In: Carlson, R.W. (Ed.), The Mantle and Core: In: Holland, H.D., Turekian, K.K. (Eds.), Treatise on Geochemistry, Vol. 2. Elsevier-Pergamon, Oxford. 171–275 pp.

Rudnick, R.L., 1992. Xenoliths — samples of the lower continental crust. In: Fountain, D.M., Arculus, R., Kay, R.W. (Eds.), Continental Lower Crust. Elsevier, pp. 269–316.

Saadat, S., Stern, C.R., 2011. Petrochemistry and genesis of olivine basalts from small monogenetic cones of Bazman stratovolcano, Makran arc, southeastern Iran. Lithos 125, 607–619.

Saadat, S., Karimpour, M.H., Stern, C.R., 2010. Petrochemical characteristics of Neogene and Quaternary alkali olivine basalts from the western margin of the Lut block, eastern Iran. Iranian Journal of Earth Sciences 2, 87–106.

Saunders, A.D., Tarney, J., 1984. Geochemical characteristics of basaltic volcanism within back-arc basins. In: Kokelaar, B.P., Howells, M.F. (Eds.), Marginal basin geology volcanic and associated sedimentary and tectonic processes in modern and ancient marginal basins: Special Publication of the Geological Society, pp. 59–76.

Scarrow, J.H., Cox, K., 1995. Basalts generated by decompressive adiabatic melting of a mantle plume: a case study from the Isle of Skye, NW Scotland. Journal of Petrology 36, 3–22.

Shahabpour, J., 2005. Tectonic evolution of the orogenic belt in the region located between Kerman and Neyriz. Asian Earth Sciences 24, 405–417.

Stern, C.R., Kilian, R., Olker, B., Hauri, E.H., Kyser, T.K., 1999. Evidence from mantle xenoliths for relatively thin (<100 km) continental lithosphere below the Phanerozoic crust of southernmost South America. Lithos 48, 217–235.

Sun, S.S., 1980. Lead isotopic study of young volcanogenic rocks from mid-ocean ridges, ocean islands and island arcs. Philosophical Transactions of the Royal Society of London 409–445.

Sun, S.S., McDonough, M.F., 1989. Magmatism in the ocean basins: Special Publication of the Geological Society, 42, pp. 313–345.

Tabatabai Mir, S., Bergman, E., Gheitanchi, M.R., 2008. 3-Dimensional upper mantle velocity structure for Iranian Plateau revealed by Pn and Sn tomography. Journal of the Earth and Space Physics 33 (3), 13–24.

Taylor, S.R., McLennan, S.M., 1985. The continental crust: its composition and evolution: Blackwell Scientific Publications, p. 312.

Thirlwall, M.F., J., U.B.G., Jenkins, C., 1994. Interaction between continental lithosphere and the Iceland plume Sr–Nd–Pb isotope geochemistry of Tertiary basalts, NE Greenland. Journal of Petrology 35, 839–879.

Verdel, C., 2009. I. Cenozoic Geology of Iran: An Integrated Study of Extensional Tectonics and Related Volcanism, II. Ediacaran Stratigraphy of the North American Cordillera: New Observation from Eastern California and Northern Utah. California Institute of Technology, Pasadena, California. 287 pp.

Villemant, B., Jaffrezic, H., Joron, J.L., Treuil, M., 1981. Distribution coefficients of major and trace-elements — fractional crystallization in the alkali basalt series of Chaine-Des-Puys (Massif Central, France). Geochimica et Cosmochimica Acta 45 (11), 1997–2016.

Walker, R., Jackson, J., 2004. Active tectonics and late Cenozoic strain distribution in central and eastern Iran. Tectonics 23, 24.

Walker, R., Jackson, J., Baker, C., 2004. Active faulting and seismicity of the Dasht-e-Bayaz region, eastern Iran. Geophysics Journal International 157, 265–282.

Walter, M.J., 1998. Melting of garnet peridotite and the origin of komatiite and depleted lithosphere. Journal of Petrology 39, 29–60.

Wilshire, H.G., Shervais, J.W., 1975. Al-augite and Cr-diopside ultramafic xenoliths in basaltic rocks from western United States. Physics and Chemistry of the Earth 9, 257–272.

Wilson, M., 1989. Igneous Petrogenesis: A Global Tectonic Approach. Unwin Hyman. 466 pp.

Wright, J.B., 1968. Deep crustal origin for oligoclase and andesine phenocrysts in basalt from Gombe, Nigeria. Nature 218, 262–263.